J. Earth Syst. Sci. (2020)129 31
https://doi.org/10.1007/s12040-019-1290-7

Modelling of earthquake locations and source parameters in Kachchh region to understand genesis of earthquakes

Bhoopendra Singh[1,2,*] and Prantik Mandal[2]

[1] *Academy of Scientific and Innovative Research (AcSIR), CSIR–National Geophysical Research Institute, Uppal Road, Hyderabad, India.*
[2] *CSIR–National Geophysical Research Institute, Uppal Road, Hyderabad, India.*
**Corresponding author. e-mail: bhoope6860@gmail.com*

MS received 14 June 2018; revised 17 August 2019; accepted 28 August 2019

Modelling of earthquake source locations and parameters infers seismogenesis of earthquakes. In this study, we modelled the earthquake source locations through hypocenter location algorithm using the difference in arrival time of P and S waves and source parameters through the Levenberg–Marquardt non-linear inversion method using S-wave spectra. A total of 340 aftershocks of 2001 Bhuj mainshock ($1.8 \leq M_w < 4.3$), which have occurred in Kachchh, Gujarat, India from January 2014 to January 2015, are located in this study. Out of 340 aftershocks, digital waveforms of 78 aftershocks ($2.2 \leq M_w < 3.9$) are used for estimation of the earthquake source parameters. The results obtained from earthquake locations show two clusters of seismicity along the Kachchh Mainland Fault (KMF) and North Wagad Fault (NWF) and three felt events ($M_w \geq 3.0$); one along the Katrol Hill Fault (KHF) ($M_w = 3.3$), two along the Banni Fault (BF) ($M_w = 3.0, 3.2$). The generation of these three felt events is attributed to the triggering mechanisms caused by the migration of fluids or the stress pulse generated by the 20 MPa stress drop of the M_w 7.7 Bhuj earthquake. A marked concentration of events is noticed in 15–30 km depth range, which could be attributed to the presence of a mafic intrusive body, resulting in stress build-up for earthquake generation in this region. The results of source parameters; seismic moment (M_0), source radius (r) and stress drop ($\Delta\sigma$) vary from 1.86×10^{12} to 3.2×10^{15} N m, 146–262 m and 0.04–5.73 MPa, respectively. The maximum stress drop value is estimated to be 5.73 MPa at 24 km depth for the largest studied event of M_w 3.9. Large stress drops are confined to the 8–33 km depth range, which indicates the probable existence of the base of the seismogenic layer in this depth range. This observed large stress drops could be attributed to stresses induced by crustal mafic intrusive bodies and the presence of aqueous fluids in the lower crust below the region.

Keywords. Hypocenter; source parameters; felt events; aftershocks.

1. Introduction

The Kachchh region (200 km × 300 km) is a unique intra-plate region (1000 km away from the Himalayan plate boundary in the north and 400 km away from the Herat–Chaman plate boundary in the west). This region experienced two massive (M_w 7.8 and 7.7) intraplate earthquakes namely; Allah-bund (1819) and Bhuj (2001). The 2001 Bhuj earthquake caused catastrophic damage and causalities to the state of Gujarat, killing about 14,000 persons and injuring many more

Published online: 20 December 2019

(Mishra 2004). After the occurrence of the 2001 Bhuj earthquake, a number of aftershocks occurred that includes 16 $M_w \geq 5$, over 250 $M_w \geq 4$, and 4000 $M_w \geq 3$ shocks, and 5000 other well-located shocks of moment magnitude (M_w) 1.0 to 2.9 (Mandal and Rastogi 2005; Mandal *et al.* 2009; Rastogi *et al.* 2013a, b). The nature of occurrence of these aftershocks is still not well understood. So it is necessary to understand the source process responsible for generating these aftershock sequence to reduce the seismic risk associated with them. In this study, we made an effort to understand the earthquake generation process in the Kachchh region through the modelling of earthquake locations and source parameters. Primary objectives of the present study are to identify the seismic zone through earthquake locations and constraining the scaling among the earthquake's source parameters through estimation of source parameters for small earthquakes occurring in the Kachchh rift zone.

In general, spectral properties of small earthquakes at high frequencies are analysed to determine their source parameters, which are relatively complicated. This is because of the fact that the path and site-effects of smaller earthquakes are difficult to distinguish from their source characteristics. The high-quality of the analyzed dataset and the corrections applied to the spectra made it possible to obtain reliable source parameters for earthquakes occurring in Kachchh, Gujarat, India. Several researchers studied earthquake source parameters (e.g., M_0, r and $\Delta\sigma$) in the Kachchh region (table 1). Their studies show that the stress drop values associated with Bhuj earthquakes are much higher than any other intraplate earthquakes in India. Because of this high value of stress drop, we intend to further study the source parameters specially stress drop associated with events occurring in the Kachchh rift zone.

In this study, we used broadband waveform data recorded at 12 broadband stations of the NGRI network in the Kachchh region during January 2014 to January 2015. First, we located 340 aftershock events ($1.8 \leq M_w \leq 4.3$), which are recorded at above seismic stations, using the hypocenter location algorithm. After that, we selected 78 aftershock events ($2.2 \leq M_w \leq 3.9$), that occurred during May–June 2014 for the estimation of source parameters like M_0, r and $\Delta\sigma$. These source parameters are estimated through the Levenberg–Marquardt non-linear inversion method using S-wave spectra. Further, we plotted these source parameters with respect to each other to find scaling among them. Finally, the source parameters are interpreted in terms of tectonics of the Kachchh region.

2. Geology and tectonics of the Kachchh region

Quaternary/Cenozoic sediments, Deccan volcanic and Jurassic sandstones resting on the Precambrian basement characterise the Geology of Kachchh peninsula (Biswas 1987; Gupta *et al.* 2001). Geomorphologically, the Kachchh region is classified into four major E–W trending zones: (a) Great and Little Rann of Kachchh ($\sim$2 m above mean sea level (MSL)) in the north and Little Rann in the east comprising of vast saline wasteland. (b) The Banni Plain (<5 m above MSL and marked by raised fluvio-marine sediments, mud flats and salt pans). (c) The Hilly region which is divided into three parts; first, the central portion comprising rocky upland; second, northern hill range; and third, coastal plains. (d) The Coastal Plains.

The major structural features of the study area are characterized by a rift basin and several east–west trending faults and folds. The Nagar Parkar fault (NPF) and the Kathiawar Fault

Table 1. *A review of earthquake source parameters in Kachchh seismic zone.*

Authors	Year	Seismic moment (M_0) (Nm)	Source radius (r) (m)	Stress drop ($\Delta\sigma$) (MPa)
Mandal and Johnston	2006	1.9×10^{12}–4.5×10^{17}	239–2835	0.63–20.7
Mandal and Dutta	2011	3.1×10^{13}–2.0×10^{17}	226–889	0.11–7.44
Saha *et al.*	2012	1.1×10^{12}–4.0×10^{16}	132.6–513.2	0.01–20.0
Rapolu and Mandal	2014	3.5×10^{11}–2.8×10^{17}	107–1515	0.13–26.7
Kumar *et al.*	2014	1.02×10^{14}–6.2×10^{15}	233–857	4.2–23.0
Kumar *et al.*	2015	1.5×10^{12}–2.4×10^{17}	139.1–933.9	0.1–14.4
Trivedi and Parvez	2015	2.0×10^{14}–6.3×10^{17}	168–210	6.8–29.98
Nagamani and Mandal	2017	7.03×10^{12}–5.4×10^{15}	178.6–565.2	0.53–36.79
Sairam *et al.*	2018	7.8×10^{11}–4.0×10^{16}	195–1480	4.8–10.2

(KTF) bound the Kachchh rift basin in the north and the south, respectively. Allah Bund Fault (ABF), Kachchh Mainland Fault (KMF), Katrol Fault (KF), Banni Fault (BF), and the North Wagad Fault (NWF) are the other major faults in this region. Kachchh Mainland Fault (KMF) (figure 1) and South Wagad Fault (SWF) are parts of a dextral strike-slip fault system (Biswas and Khattri 2003). South Wagad Fault is the eastward extension of Kachchh Mainland Fault (Biswas 2005). Furthermore, Kachchh Mainland Uplift, Kathiawar Uplift, Pachham, Khadir, Bela, Wagad, and Chobari uplift are several uplifts, and there are some minor NE/NW trending faults/lineaments in this region (Biswas 1987; Rastogi 2001).

3. Data and methodology

In this study, we analysed the earthquake data recorded at 12 broadband stations during January 2014–January 2015 in Kachchh rift zone, Gujarat, India. A total of 340 events ($1.8 \leq M_w \leq 4.3$) are located through the hypocenter location algorithm, using the existing velocity modal (Mandal 2007). Out of 340 events, we selected 78 events ($2.2 \leq M_w \leq 3.9$), which occurred during May–June 2014, for the estimation of source parameters. These source parameters are estimated through Levenberg–Marquardt non-linear inversion method using the best-fit S-wave spectra, which work as initial input for the Levenberg–Marquardt inversion modelling. In this inversion method, the initial value of corner frequency (f_c) and long period spectral level (Π_0) are defined from the respective observed and modelled spectra. After that the best-fit inverted spectra is obtained through iteratively minimizing the normalized difference between inverted and observed spectra using ω^{-2} source spectral model. These best-fit inverted spectra give the modal parameters (f_c and Π_0). Using these model parameters, other source parameters (M_0, r, $\Delta\sigma$, and M_w) are computed through some well-known empirical relations. According to Boatwright (1980), the

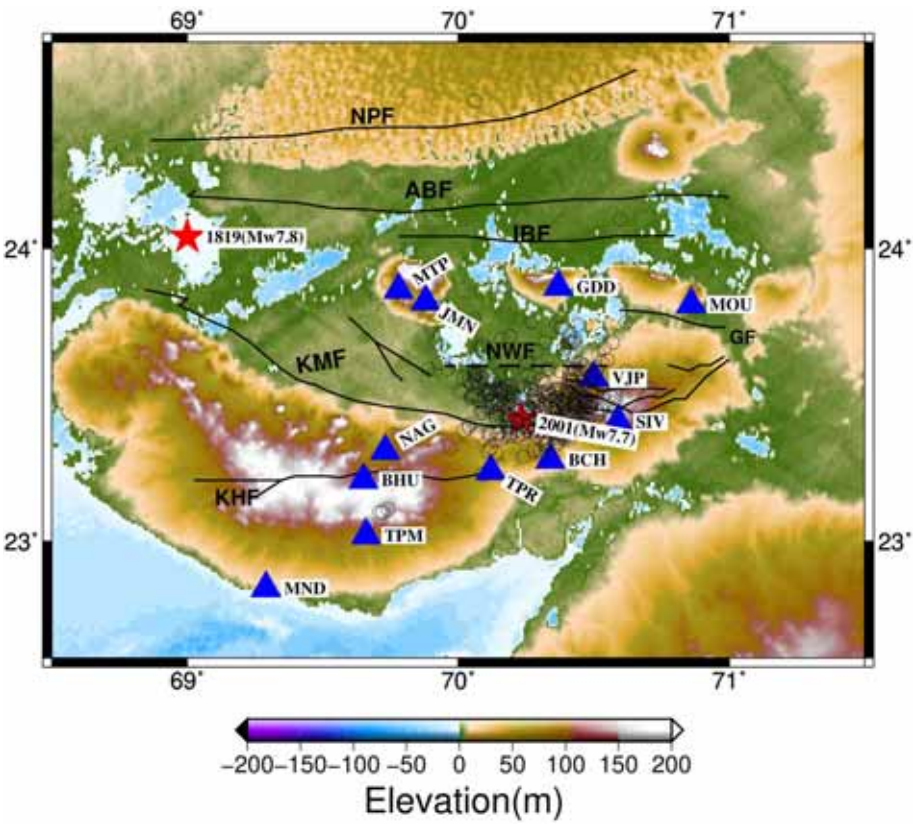

Figure 1. A plot showing the locations of seismograph stations (solid blue triangles) whose data have been used for the study of the Kachchh region, Gujarat, India. The red solid stars represent the epicenters of the 1819 (M_w 7.8) Allah-bund and 2001 (M_w 7.8) Bhuj earthquakes. Open black circles represent epicenters of the aftershocks of the Bhuj mainshock. ABF: Allah Bund Fault, IBF: Island Belt Fault, KMF: Kachchh Mainland Fault, KHF: Katrol Hill Fault, NPF: Nagar Parkar Fault, BF: Banni Fault, GF: Gedi Fault and NWF: North Wagad Fault are shown by solid black lines.

source term for S-waves (A_0) (high frequency fall-off ($\gamma = 2$)) can be written as:

$$A_0 = \frac{\Pi_0}{\left[1 + \left(\frac{f}{f_c}\right)^{2\gamma}\right]^{0.5}} = \frac{\Pi_0}{\left[1 + \left(\frac{f}{f_c}\right)^{4}\right]^{0.5}} = \frac{\Pi_0}{[B_4]^{0.5}}. \tag{1}$$

For the spectral amplitudes at a distance R from the source, with no attenuation effect, equation (1) can be written as (Fletcher 1995):

$$\ln[A(f,R)] = \ln\left\{\frac{\Pi_0}{\left[1 + \left(\frac{f}{f_c}\right)^{4}\right]^{0.5}}\right\} - \ln(R) - \frac{\omega t^*}{2}, \tag{2}$$

where $t^* = R/Q_0\ Vs$.

Q_0 and R represent the quality factor and hypocentral distance, respectively. 'R' term can be removed from equation (2), because the geometrical spreading effect is already corrected in the formula for seismic moment. Now the B_4 term can be expanded through the Taylor series. It gives roots of above nonlinear equation (Press *et al.* 1992) now, above equation (2) can be written as:

$$A(f) = \ln \Pi_0 - 0.5 \ln B_4 + 2B_4^{-1}\left(\frac{f}{f_c}\right)^4\left(\frac{\Delta f_c}{f_c}\right) - \frac{\omega t^*}{2}. \tag{3}$$

To obtain the model parameters equation (3) can be solved using a least-squares algorithm. In fact, the error can be minimized through least squares method by solving:

$$\mathrm{D} = \mathrm{GM}, \tag{4}$$

where M, G and D represent the model parameter matrix, sensitivity matrix and data matrix respectively.

$$\mathrm{M} = [\ln(\Pi_0),\ t^* Df_c]^{\mathrm{T}},$$

$$\mathrm{G} = \left[1, -\frac{\omega}{2}, 2B_4^{-1}\left(\frac{f}{f_c}\right)^4 \Big/ f_c\right], \tag{5}$$

$$\mathrm{D} = [\ln A(f) + 0.5 \ln B_4].$$

Newton's method for quasi-linear equation can be written as:

$$\Delta\mathrm{M} = \left(\mathrm{G}^{\mathrm{T}}\mathrm{G}\right)^{-1}\mathrm{G}^{\mathrm{T}}\Delta\mathrm{D}, \tag{6}$$

where, ΔM and ΔD represent the change in model parameters and the difference between predicted data and observed data, respectively. The solution is obtained iteratively through $M_k = M_0 + M_{k-1}$ equation where M_0 represent the initial model. The Lavenberg–Marquardt inversion technique is used to estimate $\ln \Pi_0$ and f_c with 10 iterations, because sensitivity matrix tends to singular. Now, equation (6) can be written as:

$$\Delta\mathrm{M} = \left(\mathrm{G}^{\mathrm{T}}\mathrm{G} + \lambda I\right)^{-1}\mathrm{G}^{\mathrm{T}}\Delta\mathrm{D}, \tag{7}$$

where λ and I are the Levenberg–Marquardt adjustable damping parameter and the identity matrix, respectively. In this inversion method, first, the initial guessed value of Δf_c is set 0.1 Hz for all events, and spectral level (Π_0) is selected from the respective low-frequency spectral level. The initial guessed value of t^* is estimated though the equation $t^* = R/Q_0 V_s$, where R is the hypocentral distance (km) and $Q_0 = 102$ (Mandal *et al.* 2004a), while $V_s = 3.5$ km/s (Mandal 2007) for the Kachchh region. After that we estimated the normalized difference between the computed spectra and that yielded from equation (1) at each iteration. The maximum difference is selected on the basis of initial guessed values of Π_0, t^* and f_c, and the minimum value is based on the accuracy of the Π_0, t^* and f_c values that can be expected to obtain from the inversion of noisy data (Mandal and Dutta 2011). An initial value of $\lambda = 0.001$ is also assigned. After that initial guessed values are substituted into equation (7) to estimate the change in model parameter (ΔM). In the next iterations, a new model parameter is estimated through $M_{r+1} = M_r + DM_r$ equation, where M_r and DM_r represent the model parameters and change in parameter values at the r^{th} iteration, respectively. The best fit model which provides the model parameters, i.e., f_c, t^* and Π_0 is obtained after 10 iterations. In this study, the damping factor λ, vary from 1 to 300. Source parameters like M_0, r and $\Delta\sigma$ are estimated using model parameters obtained from the above inversion technique, through following empirical relations (Keilis-Borok 1959; Brune 1970):

$$M_0 = \frac{4\pi\rho V_s^3 R\Pi_0}{FR_{\theta\phi}}, \tag{8}$$

$$r = \frac{2.34 * V_s}{2\pi f_c}, \tag{9}$$

$$\Delta\sigma = \frac{7}{16} * \left(\frac{M_0}{r^3}\right), \tag{10}$$

where Π_0, f_c, V_s, R and 'ρ' represent the long-period spectral level (m/s), corner frequency (Hz), the S-wave velocity (m/s), hypocentral distance (m) and rock density (kg/m^3), respectively. The value of mean radiation pattern, $R_{\theta\phi}$ is 0.55 for the Kachchh region (Mandal and Johnston 2006). And free surface correction factor (F) assumed 2 for the study region. The estimated M_0, r and stress drop are in N m, m, and Pa, respectively (1 MPa = 10^6 Pa). And, M_w is estimated using the following equation:

$$M_w = \frac{2}{3}\log_{10}(M_0) - 6.06. \tag{11}$$

4. Error analysis

The error in source parameters are analyzed by estimating the standard deviation and mean of M_0, r and $\Delta\sigma$. The average (M_0) and (r) are estimated through the following equation (Archuleta *et al.* 1982):

$$\langle M_0\rangle = \text{antilog}\left[\left(\frac{1}{NS}\right)\sum \log M_{0i}\right], \tag{12}$$

and

$$\langle r\rangle = \left[\left(\frac{1}{NS}\right)\sum r_i\right]. \tag{13}$$

The standard deviations (σ) of the log moment are estimated through the following equation,

$$\text{sd}(\log\langle M_0\rangle) = \left\{\left(\frac{1}{NS} - 1\right) * \sum[\log M_{0i} - \log\langle M_{0i}\rangle]^2\right\}^{0.5}. \tag{14}$$

Multiplicative error factors are estimated using equation as given below

$$E_{mo} = \text{antilog}\{\text{sd}(\log\langle M_0\rangle)\}. \tag{15}$$

Similarly, average and the standard deviation for r and f_c are calculated. Finally, the standard deviations of $\Delta\sigma$ are estimated using the following equation (Fletcher *et al.* 1984):

$$\sigma_{\text{std}} = \Delta\sigma\left\{\left(\frac{\sigma_m}{M_0}\right)^2 + 9\left(\frac{\sigma_r}{r}\right)^2\right\}^{0.5}. \tag{16}$$

5. Computation of earthquakes source locations and source parameters

Earthquakes source locations (hypocenters) are determined by picking P phase from vertical component and S phases from radial or transverse component of seismogram (figure 2). Hypocenter location algorithm is used to locate these source locations. Error in hypocenter is determined by the method of Jordan and Sverdrup (1981). For computation of source parameters, an instrumental correction is applied to the waveform data of selected 78 aftershocks using pole-zero files of the sensor through the inbuilt 'transfer' facility of Seismic Analysis Code (SAC) (2000). Mean and trend are removed from waveform data using SAC. A time window of 5.12 s is chosen from beginning of the S-arrival. After that a 5% cosine tapering on both sides is applied. Finally, the S-wave spectra are computed through Fast Fourier Transform (FFT). These S spectra are used for estimation of f_c and Π_0 which are used for computation of other source parameters (M_0, r, $\Delta\sigma$ and M_w). The errors in source parameters are computed through estimation of the standard deviation of source parameters (figure 3).

6. Results and discussions

6.1 *Earthquake locations*

Seismicity of the Kachchh region during January 2014–January 2015 has been monitored using the 12 broadband seismic network of NGRI, Hyderabad (figure 1). A total of 340 earthquake hypocentral locations are shown in figure 4 (table A1). Error in hypocenter varies from 0.5 to 2.6 km in latitude, 0.4 to 2.3 km in longitude and 0.7 to 4.7 km in focal depth. Two clusters of seismicity are seen along the KMF and NWF. Moment magnitude (M_w) of these selected events range from 1.8 to 4.3 while focal depth varies from 2.0 to 4.7 km. We divided these located event magnitudes into three ranges $M_w < 2.0$, $2.0 \le M_w < 3.0$, and $3.0 \le M_w < 4.5$. We found that the majority of events lie in $M_w \ge 2.0$ range (337 events), not in $M_w < 2.0$ range (three events). Theoretically, the occurrence of smaller events ($M_w < 2.0$) should be more in comparison to the occurrence of $M_w \ge 2.0$. Thus, our above observation regarding fewer occurrences of smaller events ($M_w < 2.0$) may be because of the event detection sensitivity of our

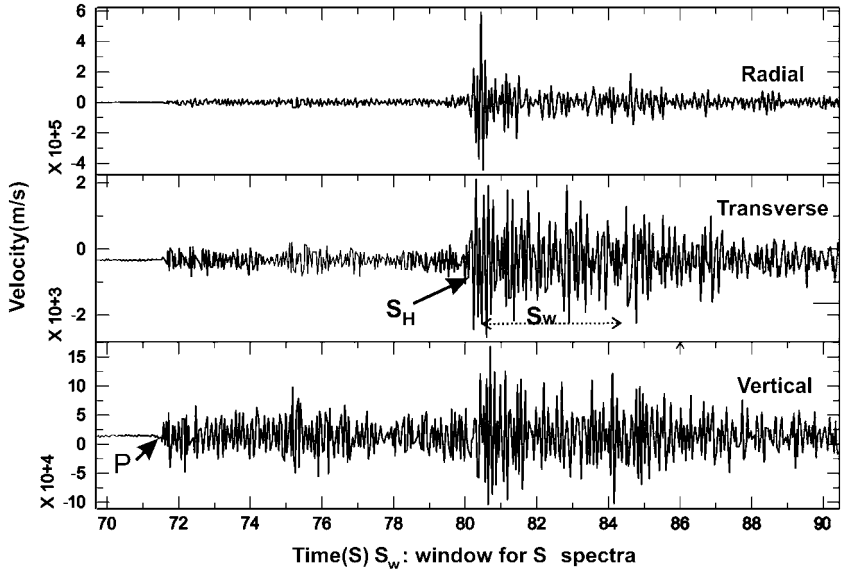

Figure 2. A plot showing three-component seismograms recorded at NGRI network in Kachchh, Gujarat, India.

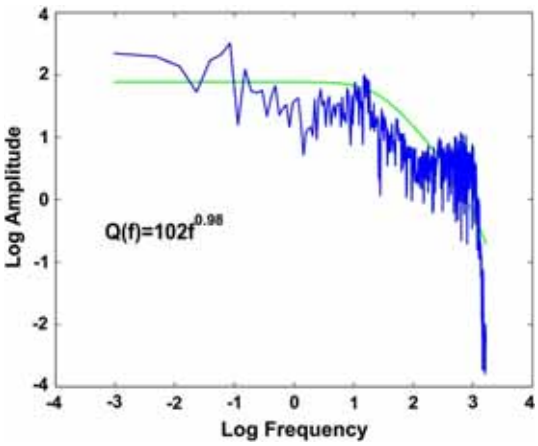

Figure 3. Plot showing S-wave spectra fitting through the Levenberg–Marquardt non-linear inversion method.

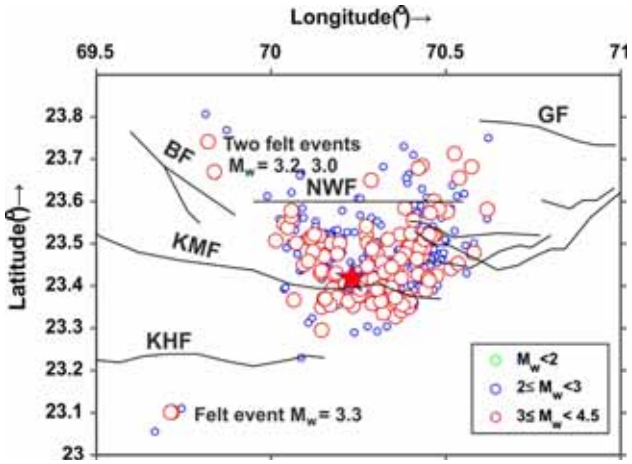

Figure 4. Epicentral plot of earthquakes in Kachchh during January 2014–January 2015. The epicenters of shocks of $M_w < 2.0$, $2.0 \le M_w < 3.0$, and $3.0 \le M_w < 4.5$ are shown by small, medium and large circle, respectively. Red star shows the 2001 Bhuj earthquake. Dark solid lines show different faults in the Kachchh region.

network. Most of the felt events $M_w \ge 3.0$ occurred along the KMF and NWF. However, three felt events ($M_w \ge 3.0$) took place along different faults, away from the main seismic clusters; one along the KHF ($M_w = 3.3$), two along the BF ($M_w = 3.0, 3.2$). Additionally, there are few smaller events around the Bhuj aftershock zone. Several mainshocks ($4.4 \le M_w \le 5.6$) are reported along different faults during 2006–2012 (Rastogi *et al.* 2014). The total number of such mainshocks is at least 20 in Kachchh, e.g., an M_w 5.6 earthquake in March 2006 along the GF about 75 km northeast of the 2001 mainshock epicentre, an M_w 4.4 shock of October 28, 2009, along with the Gora Dungar Fault, and an M_w 5.1 shock of June 19, 2012, along a transverse fault north of the rupture zone of the 2001 Bhuj mainshock (Rastogi *et al.* 2014). The generation of a large number of main shocks is attributed to the triggering mechanisms caused by migration of fluids or the stress pulse generated by the 20 MPa stress drop of the M_w 7.7 Bhuj earthquake in 2001 (Mandal *et al.* 2016; Rastogi *et al.* 2013b). This stress pulse migrates to distances of 100–200 km and even 6–16 yrs after the Bhuj earthquake. This triggered seismicity may be because of an increase in Coulomb stress of up to 1 bar in Kachchh, has estimated by viscoelastic modelling (Rastogi *et al.* 2013b). Note that Scholz

(1977) gave the explanation of the Haicheng earthquake prediction by propagation of the deformation front at a rate of 110 km/year and explained that this might result from stress pulse migration through the mantle (Savage 1971; Bott and Dean 1973). The epicentral plot and depth sections of located aftershocks are shown in figures 4 and 5, respectively. In-depth sections, no earthquakes are noticed in the top (0–2 km depth). This can be attributed to the unconsolidated sediments of the Kachchh basin, which does not host favourable environment for accumulating stresses, thereby, generating earthquakes. A marked concentration of events is noticed in 15–30 km depth range, which could be attributed to the presence of a mafic intrusive body, resulting in stress build-up for earthquake generation in this region (Mandal *et al.* 2004b). Note that the rheological modelling of the Kachchh region reveals a deeper brittle/ductile transition zone at 25 km depth, suggesting the brittle crust extending down to 35 km depth, which suggests the possibility of occurrence of earthquakes down to 35 km depth (Mandal and Pandey 2010).

6.2 *Earthquake source parameters*

Source parameters are estimated for 78 aftershocks ($2.2 \leq M_w \leq 3.9$), which occurred during May–June 2014. The hypocentral parameters of these events are given in table A2. The estimated source parameters like M_0, r and $\Delta\sigma$ vary from 1.86×10^{12} to 3.2×10^{15} N m, 146 to 262 m and 0.04 to 5.73 MPa, respectively (table A3). The maximum stress drop value is estimated to be 5.73 MPa at 24 km depth for the event of M_w 3.9. The seismic moment (M_0) *vs.* corner frequency (f_c) plot (figure 6a) shows that corner frequency (f_c) is decreasing with increasing seismic moment (M_0), following a linear relationship. This relation can be written as $M_0 = 7 \times 10^{24}\, f_c - 12.6$. The estimated values of the seismic moment are plotted against source radius in logarithmic scale with the constant stress drop lines (figure 6b). This plot shows that the source radii are weakly dependent on the size of event. Our estimated logarithmic $\Delta\sigma$ values also show a linear relation with logarithmic of the M_0 (figure 6c), which can be written as $[\mathrm{Log}_{10}(\Delta\sigma) = 0.722 \log_{10}(M_0) - 10.34]$. Stress drops as a function of earthquake size have also been observed by Bodin *et al.* (2004) for their ground motion scaling study of the Kachchh basin. In general, stress drop

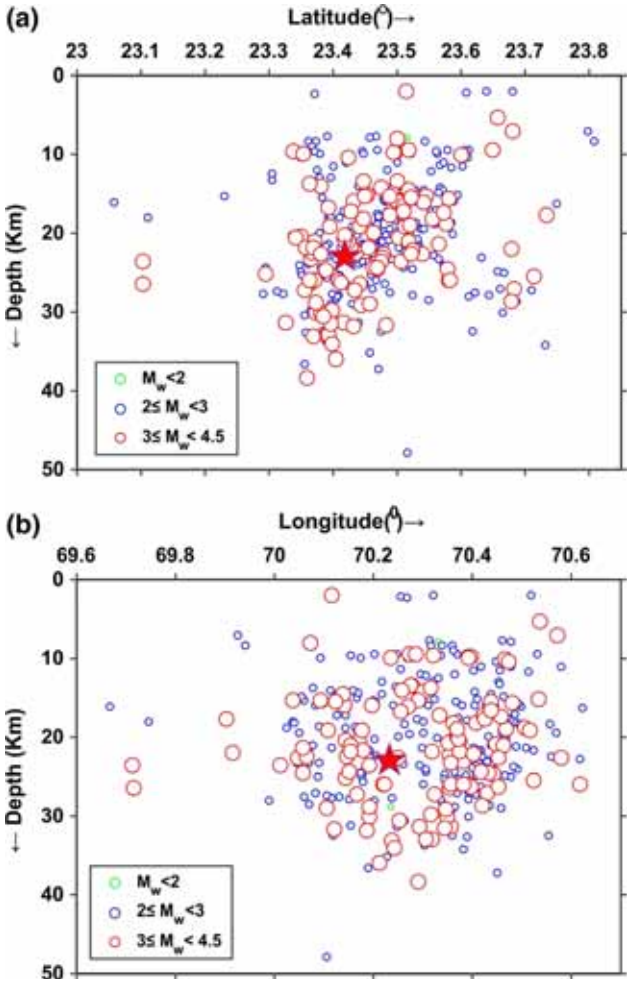

Figure 5. (**a**) E–W depth plot of located aftershocks during January 2014–January 2015. (**b**) N–S depth plot of located aftershocks during January 2014–January 2015. The epicenters of shocks of $M_w < 2.0$, $2.0 \leq M_w < 3.0$, and $3.0 \leq M_w < 4.5$. are shown by small, medium and large circles, respectively, and a red star shows the 2001 Bhuj earthquake in both (a and b).

does depend on the size of earthquake (Aki 1962). It is also seen from the plot between M_0 and r (figure 6b). But, Toro and Silva (2001) proposed that stress drop, in general, independent from the size of earthquake. However, some researchers documented about the earthquake scaling in terms of M_0 and $\Delta\sigma$ (Archuleta *et al.* 1982; Mayeda and Walter 1996). The depth-wise plot of stress drop hardly shows any variation in stress drop with depth (figure 6d). Note that all known larger ($M \geq 7$) stable continental intra-plate earthquakes took place in failed rifted crust (Johnston 1994). In general, it is observed that the stress drops for intra-plate earthquakes is higher than inter-plate earthquakes (Kanamori and Allen 1986). To characterize the continued aftershock activity in Kachchh region, we compared our source

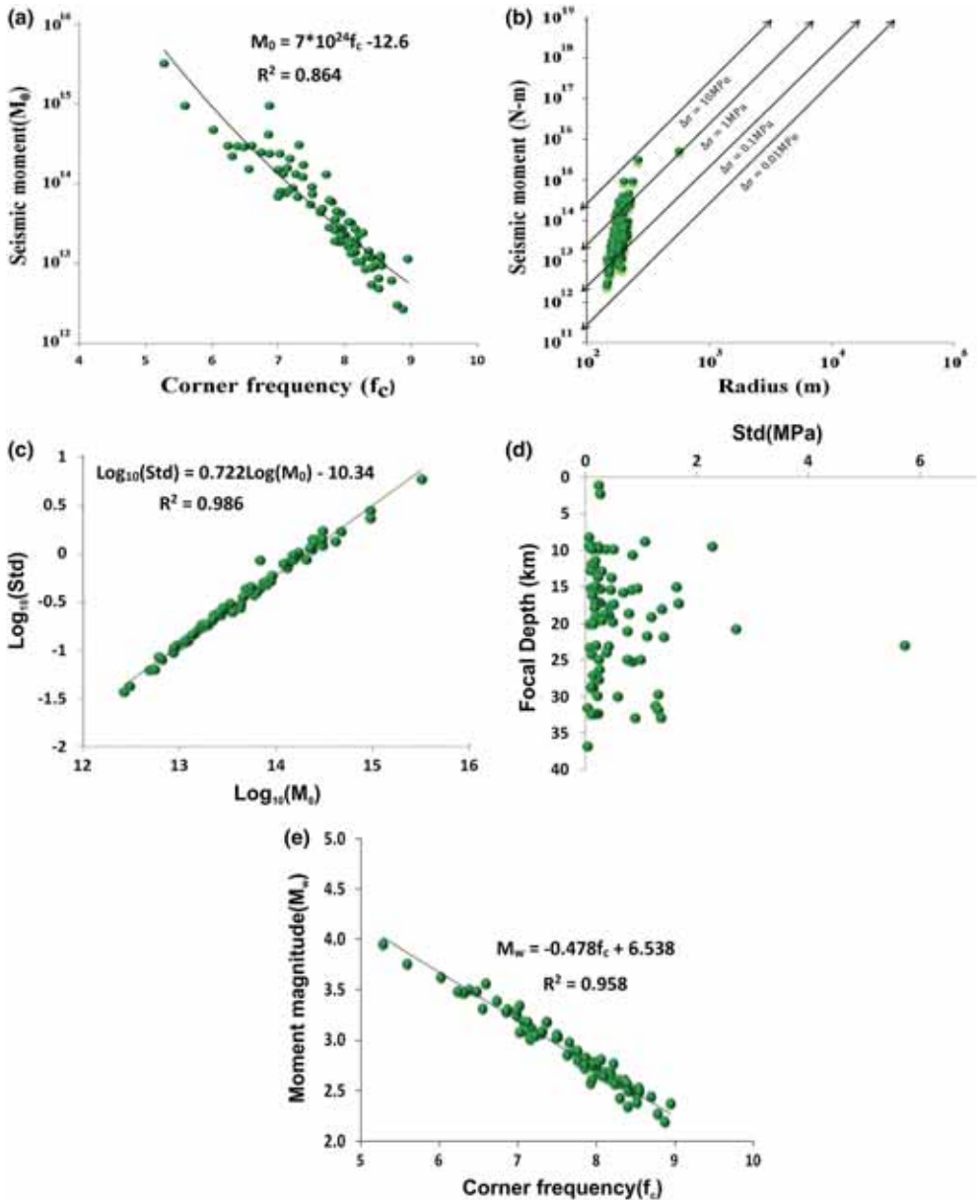

Figure 6. (**a**) Plot of corner frequencies (f_c) with seismic moment (M_0). (**b**) Estimated (M_0) is plotted against the source radius (r) with the constant stress ($\Delta\sigma$) drop lines. (**c**) Plot of stress drop (std) with seismic moment (M_0) in log–log scale. (**d**) Plot between stress drop ($\Delta\sigma$) and focal depth (km). (**e**) Plot between moment magnitude (M_w) and corner frequency (f_c).

parameter's results with previous source parameter's studies in Kachchh region, those of aftershocks of other large intraplate and interplate events of India. The large stress drops estimated for the Bhuj earthquake (2001) of M_w 7.7 about ∼21 MPa (Antolik and Dreger 2003) and the Latur earthquake (1993) of M_w 6.3 about ∼7 MPa (Baumbach *et al.* 1994). These earthquakes are classified as intra-plate earthquakes according to the stress drop estimates as provided by Scholz *et al.* (1986). For the M_w 5.8 Jabalpur earthquake and M_w 5.7 Bhuj aftershock, Singh *et al.* (1999) have reported a static stress drop of 20 and 3.5 MPa, respectively. The source parameters for the Koyna earthquake sequence (1994–1997) show that the value of stress drops vary from 0.03 to 19 MPa for events of M_w 1.5 to 4.7 (Mandal *et al.* 1998). While the stress drops of the interplate Uttarkashi (1991) of M_w 6.8 and Chamoli (1999) of M_w 6.5 are found to be 4 and 15 MPa, respectively (Singh *et al.* 2004). The ground motion prediction study for Kachchh basin by Bodin *et al.* (2004) suggests that the stress drops range from 0.07 to 100 MPa for the Bhuj aftershocks of M_w ranging

from 2 to 5.2. Moreover, the present study reveals a stress drop variation from 0.04 to 5.73 MPa for the Bhuj aftershocks ($2.2 \leq M_w \leq 3.9$). Thus, it seems that our stress drops estimates are in good agreement with those estimates of other Indian intraplate earthquakes (as discussed above), whereas, Bodin *et al.* (2004)'s and other previous stress drop estimates in Kachchh region seem to be overestimated or these higher values of stress drops have been attributed to the crustal mafic intrusive bodies and the presence of aqueous fluids in the lower crust (Mandal and Johnston 2006). Figure 6(e) shows that corner frequencies decrease with the increasing moment magnitude values followed by a linear relation given by $M_w = -0.478 f_c + 6.538$. The standard deviations of (M_0, f_c, r and $\Delta\sigma$) are listed in table A3 for the aftershocks recorded at two or more stations. The standard deviations (σ) of (f_c, $\log(M_0)$, r and $\Delta\sigma$) are found to be varying from 0.13 to 1.93 Hz, 0.05 to 1.50 N m, 2.13 to 63.32 m, and 0.01 to 4.46 MPa, respectively while the error factor E_{mo} for seismic moment is estimated to be ranging from 0.23 to 4.47. The estimated $\sigma_{f_c}, \sigma_{\log(M_0)}, \sigma_r$ and σ_{std} for the whole dataset is 0.77 Hz, 0.26 N m, 21.17 m and 0.80 MPa with an average values 7.66 Hz, 0.54 N m, 172.94 m and 0.59 MPa, respectively.

7. Conclusions

The epicentral plot of aftershocks show two clusters of seismicity along the KMF and NWF and three felt events; one along the KHF and two along the Banni Fault. These three felt events could be occurred due to triggering caused by migration of fluids or the stress pulse generated by the 20 MPa stress drop of the M_w 7.7 Bhuj earthquake in 2001. This triggered seismicity may also be because of an increase in Coulomb stress of up to 1 bar in Kachchh. A marked concentration of events is noticed at 15–30 km depths, which could be attributed to the presence of a crustal mafic intrusive body, resulting in stress build-up for earthquake generation in this region. Our estimates of M_0, r and $\Delta\sigma$ for the aftershocks ($2.2 \leq M_w \leq 3.9$) vary from 1.86×10^{12} to 3.2×10^{15} N m, 146 to 262 m and 0.04 to 5.73 MPa, respectively. The maximum stress drop value is estimated to be 5.73 MPa at 24 km depth for the largest studied event of M_w 3.9. These estimated source parameters are also used to derive probable source scaling of intraplate earthquakes occurring in the Kachchh region. The scaling between M_0 and f_c, M_0 and $\Delta\sigma$ and M_w and f_c can be seen from linear equations $M_0 = 7 \times 10^{24} f_c - 12.6$, $\text{Log}_{10}(\Delta\sigma) = 0.722 \log_{10}(M_0) - 10.34$ and $M_w = -0.478 f_c + 6.538$, respectively. Large stress drops are confined to the 8–33 km depth range, which indicate the probable existence of the base of the seismogenic layer in this depth range. The observed large stress drops in the 8–33 km depth range could be attributed to stresses induced by crustal mafic intrusive bodies and the presence of aqueous fluids in the lower crust below the region, as revealed by the earlier tomographic studies. The standard deviations (σ) of (f_c, $\log(M_0)$, r and $\Delta\sigma$) are found to be varying from 0.13 to 1.93 Hz, 0.05 to 1.50 N m, 2.13 to 63.32 m, and 0.01 to 4.46 MPa, respectively. While the error factor E_{mo} for seismic moment is estimated to be ranging from 0.23 to 4.47. The estimated $\sigma_{f_c}, \sigma_{\log(M_0)}, \sigma_r$ and σ_{Std} for the whole dataset are 0.77 Hz, 0.26 N m, 21.17 m and 0.80 MPa with an average value 7.66 Hz, 0.54 N m, 172.94 m and 0.59 MPa, respectively.

Acknowledgements

The authors are grateful to the Director, Council of Scientific and Industrial Research–National Geophysical Research Institute (CSIR–NGRI), Hyderabad, India, for his kind permission to publish this work. This study is also supported by the Council of Scientific and Industrial Research (CSIR) 12 Five-Year-Plan Project (Heart) at the CSIR–NGRI, in Hyderabad. BS is thankful to CSIR for providing a Senior Research Fellow (SRF) Fellowship for conducting this research at the Academy of Scientific and Innovative Research (AcSIR)–NGRI.

Appendix

Table A1. *Locations of Bhuj aftershocks which have occurred during January 2014 to January 2015.*

Sl. no.	Date (yymmdd)	Time (hhmm)	Time Sec	Latitude (°)	Error	Longitude (°)	Error	Depth (km)	Error	M_w	RMS	GAP
1.	140101	1423	40.45	23.679	1.9	69.915	1.9	22.0	3.9	3.2	0.02	148
2.	140102	300	35.83	23.506	0.6	70.013	0.7	23.6	2.8	3.4	0.04	94
3.	140102	853	35.83	23.379	0.9	70.281	0.5	10.0	1.4	2.9	0.04	90
4.	140103	1450	33.54	23.492	1.0	70.462	0.9	14.9	2.3	2.9	0.05	107
5.	140103	1649	46.54	23.505	0.7	70.14	0.8	16.0	1.6	3.1	0.09	102
6.	140103	1931	06.43	23.365	1.0	70.189	0.8	29.8	1.5	3.0	0.05	87
7.	140106	2350	32.35	23.519	1.1	70.486	0.9	16.1	1.9	1.9	0.03	110
8.	140107	1052	06.33	23.455	0.9	70.292	0.7	23.6	2.2	2.5	0.05	101
9.	140107	1549	38.34	23.478	1.2	70.579	1.2	22.6	2.7	3.6	0.03	134
10.	140107	2308	31.32	23.547	0.6	70.06	0.9	15.3	3.1	2.2	0.04	101
11.	140108	741	0.91	23.29	1.1	70.237	0.7	27.7	1.1	2.2	0.04	148
12.	140108	1042	4.59	23.393	1.2	70.403	0.9	21.4	2.0	2.7	0.07	122
13.	140108	1539	13.49	23.42	1.1	70.479	0.9	11.1	3.2	2.4	0.02	127
14.	140108	2043	34.88	23.448	1.1	70.234	0.8	28.8	1.8	1.8	0.08	98
15.	140110	1837	39.61	23.305	1.5	70.276	0.8	13.2	2.0	2.7	0.03	134
16.	140111	1906	19.86	23.443	1.3	70.434	0.9	23.4	2.9	2.8	0.05	105
17.	140112	1650	39.61	23.462	1.1	70.432	0.8	20.0	2.8	2.9	0.04	103
18.	140113	1021	31.66	23.587	1.1	70.467	1.0	20.1	3.8	2.7	0.03	124
19.	140113	1504	36.93	23.518	0.9	70.274	0.7	9.4	2.5	3.4	0.05	111
20.	140113	1723	54.38	23.471	1.2	70.489	1.0	18.1	2.3	2.9	0.03	113
21.	140113	2248	7.21	23.472	1.2	70.57	1.1	19.4	1.7	2.4	0.02	126
22.	140114	1329	30.97	23.528	0.8	70.218	0.9	14.5	2.5	2.5	0.07	110
23.	140114	1959	11.75	23.464	0.8	70.176	0.8	25.0	2.4	2.6	0.04	98
24.	140116	910	27.04	23.481	0.9	70.116	0.6	21.4	3.4	2.8	0.05	103
25.	140117	1340	21.14	23.516	0.6	70.33	0.9	07.9	1.9	1.9	0.03	119
26.	140119	1706	51.47	23.573	0.8	70.492	1.0	24.0	2.4	2.3	0.07	97
27.	140121	2014	15.75	23.543	2.6	70.419	1.4	22.5	2.0	2.9	0.04	173
28.	140122	1949	8.00	23.495	0.9	70.446	0.9	16.0	1.1	2.3	0.06	107
29.	140122	2102	35.28	23.349	1.3	70.144	0.5	20.4	2.1	3.0	0.02	88
30.	140123	0011	11.44	23.514	1.0	70.384	1.0	22.3	2.0	2.2	0.09	114
31.	140123	0436	54.75	23.464	1.0	70.261	0.8	23.4	2.4	2.8	0.05	106
32.	140123	0446	47.22	23.504	1.1	70.196	0.9	15.8	2.3	2.3	0.04	110
33.	140125	1454	31.64	23.612	0.8	70.531	0.8	9.4	1.1	2.9	0.11	126
34.	140126	1452	26.94	23.458	0.7	70.167	0.5	19.2	2.3	2.5	0.03	96
35.	140128	0630	18.63	23.394	0.8	70.038	0.5	18.0	2.3	2.5	0.08	79
36.	140128	1012	30.06	23.395	0.8	70.04	0.5	18.2	2.3	2.6	0.08	80
37.	140129	0220	2.62	23.507	0.8	70.499	0.9	16.1	1.2	2.4	0.09	92
38.	140129	1541	58.94	23.501	0.9	70.452	0.8	13.0	1.7	2.2	0.10	104
39.	140129	1932	26.31	23.546	0.5	70.037	0.5	15.3	1.8	3.0	0.07	98
40.	140130	1829	05.06	23.578	0.7	70.202	0.6	9.5	1.8	2.4	0.10	119
41.	140130	1943	44.43	23.611	0.8	70.447	0.7	10.4	1.6	2.8	0.09	129
42.	140131	1438	4.96	23.362	1.0	70.411	0.8	23.9	1.4	2.6	0.05	144
43.	140131	1504	37.95	23.683	0.8	70.431	0.8	27.1	1.6	3.5	0.09	145
44.	140131	1521	37.21	23.687	0.8	70.434	0.8	28.7	1.2	2.8	0.07	146
45.	140131	2354	14.58	23.567	0.6	70.255	0.6	11.4	4.7	2.1	0.06	119
46.	140201	6	34.87	23.527	0.7	70.239	0.6	15.9	1.6	2.5	0.07	111
47.	140201	59	40.17	23.683	0.9	70.413	0.7	21.8	1.9	2.5	0.05	145
48.	140201	236	35.19	23.6	0.7	70.465	0.7	10.1	1.2	3.0	0.09	127
49.	140201	440	55.99	23.404	1.2	70.34	1.0	28.3	1.1	2.7	0.03	143
50.	140201	1003	56.43	23.476	0.7	70.483	0.8	23.7	1.2	2.9	0.06	90

Table A1. *(Continued.)*

Sl. no.	Date (yymmdd)	Time (hhmm)	Time Sec	Latitude (°)	Error	Longitude (°)	Error	Depth (km)	Error	M_w	RMS	GAP
51.	140201	2300	37.78	23.44	0.7	70.141	0.5	14.0	2.4	2.7	0.03	92
52.	140202	1446	49.24	23.5	0.7	70.394	0.7	09.5	1.5	2.7	0.07	109
53.	140203	1140	8.03	23.534	0.5	70.069	0.5	21.4	2.4	2.5	0.05	100
54.	140204	655	50.69	23.392	1.0	70.358	0.8	18.0	1.8	2.6	0.03	102
55.	140205	2251	48.97	23.441	0.8	70.165	0.5	18.6	2.6	2.6	0.03	94
56.	140206	904	55.7	23.469	0.7	70.471	0.8	17.6	1.3	2.7	0.06	94
57.	140206	1336	10.79	23.373	0.9	70.338	0.8	08.4	1.8	2.2	0.07	97
58.	140206	1601	11.88	23.48	0.7	70.276	0.7	15.9	1.5	2.4	0.05	105
59.	140207	144	28.14	23.359	1.0	70.391	0.7	26.9	1.3	2.7	0.04	135
60.	140207	444	11.63	23.502	0.6	70.171	0.5	20.5	2.4	3.2	0.04	103
61.	140207	2240	54.01	23.466	0.9	70.417	0.9	21.6	1.8	2.8	0.10	93
62.	140210	1104	32.11	23.558	0.9	70.617	1.1	22.7	1.2	2.5	0.03	149
63.	140212	236	19.62	23.392	1.0	70.371	0.8	17.5	1.9	2.8	0.07	109
64.	140214	1444	6.71	23.529	0.5	70.18	0.5	18.7	2.6	2.5	0.04	108
65.	140215	139	55.22	23.573	0.8	70.418	0.7	11.1	1.6	2.9	0.08	122
66.	140215	449	3.66	23.51	0.9	70.497	0.9	18.4	1.2	2.4	0.07	93
67.	140215	1732	21.4	23.39	0.7	70.313	0.5	07.7	1.8	2.7	0.07	88
68.	140216	1218	44.8	23.501	0.5	70.277	0.5	13.4	2.6	3.7	0.03	108
69.	140217	449	12.01	23.64	0.7	70.518	0.8	02.0	0.9	2.5	0.12	133
70.	140220	1024	13.56	23.323	1.0	70.116	0.7	27.7	1.4	2.6	0.10	78
71.	140223	1615	51.65	23.497	0.8	70.393	0.9	09.7	1.8	3.1	0.11	109
72.	140224	900	16.04	23.459	0.9	70.386	0.9	25.3	1.8	2.8	0.11	98
73.	140225	1247	56.62	23.449	0.9	70.353	0.8	22.3	1.9	3.2	0.09	100
74.	140226	557	45.81	23.356	1.0	70.189	0.7	36.6	1.5	2.9	0.07	92
75.	140226	749	57.18	23.444	0.9	70.441	0.9	23.7	1.6	2.9	0.10	105
76.	140226	1025	34.16	23.478	0.8	70.299	0.6	15.6	1.8	2.5	0.07	105
77.	140227	2316	21.88	23.576	0.7	70.505	0.7	18.8	1.1	3.3	0.09	120
78.	140228	1119	59.12	23.494	0.7	70.396	0.9	09.7	1.6	3.2	0.10	108
79.	140228	1440	32.35	23.389	0.9	70.442	0.9	24.7	1.4	3.1	0.07	139
80.	140228	1444	44.85	23.391	1.0	70.434	0.9	22.9	1.6	2.9	0.09	135
81.	140228	1615	59.3	23.431	0.6	70.14	0.5	16.0	1.1	3.7	0.05	91
82.	140301	556	35.53	23.462	0.9	70.488	1.1	21.2	1.6	2.7	0.09	98
83.	140303	1319	49.69	23.519	0.6	70.139	0.6	14.5	1.9	3.3	0.07	104
84.	140303	1759	45.19	23.294	1.1	70.305	0.7	24.3	1.3	2.7	0.05	132
85.	140303	2209	12.92	23.389	1.1	70.412	1.0	21.6	1.8	2.5	0.13	128
86.	140304	457	24.22	23.513	0.5	70.109	0.4	19.2	2.5	3.4	0.04	100
87.	140305	214	46	23.373	1.1	70.191	0.7	30.0	1.7	3.3	0.09	87
88.	140305	1410	8.78	23.445	1.0	70.508	1.1	21.4	1.5	2.0	0.09	108
89.	140305	2355	32.25	23.471	1.2	70.45	2.0	37.3	1.7	2.3	0.03	180
90.	140306	148	26.78	23.664	1.0	70.393	0.9	30.0	2.0	3.0	0.10	142
91.	140306	1858	1.72	23.389	1.0	70.303	0.8	33.7	1.6	2.1	0.08	89
92.	140307	803	58.34	23.408	1.0	70.336	0.9	27.9	1.4	2.9	0.11	90
93.	140307	2226	18.6	23.407	1.0	70.202	0.7	28.0	1.6	2.5	0.11	91
94.	140307	2307	14.29	23.461	1.0	70.343	1.0	24.7	2.3	2.8	0.12	103
95.	140308	1535	46.88	23.429	0.8	70.56	0.9	22.4	1.1	2.9	0.07	110
96.	140308	1901	9.26	23.359	1.0	70.291	0.7	38.4	0.7	4.3	0.06	84
97.	140309	529	37	23.538	0.5	70.051	0.5	19.4	2.7	2.5	0.05	98
98.	140310	1348	18.54	23.404	0.9	70.439	0.9	23.3	1.4	2.4	0.08	129
99.	140311	459	18.18	23.607	0.9	70.247	0.8	09.5	2.5	2.9	0.15	127
100.	140314	2013	46.23	23.468	0.8	70.46	1.1	07.7	2.4	2.4	0.13	95
101.	140315	112	38.24	23.447	0.6	70.275	0.5	13.4	2.5	3.0	0.04	99
102.	140315	2108	19.24	23.413	1.0	70.364	0.8	21.8	1.9	2.5	0.07	98

Table A1. *(Continued.)*

Sl. no.	Date (yymmdd)	Time (hhmm)	Time Sec	Latitude (°)	Error	Longitude (°)	Error	Depth (km)	Error	M_w	RMS	GAP
103.	140319	334	51.04	23.667	0.7	70.087	0.6	25.0	2.4	2.9	0.06	129
104.	140322	118	46.73	23.396	1.0	70.465	1.1	18.0	1.8	2.9	0.12	141
105.	140322	510	47.42	23.567	0.9	70.405	1.0	14.2	2.2	2.9	0.17	121
106.	140322	1329	53.23	23.469	0.9	70.433	0.9	24.5	1.6	3.5	0.10	92
107.	140324	428	45.96	23.496	1.0	70.557	1.2	18.3	1.6	2.7	0.14	119
108.	140324	917	36.3	23.539	0.5	70.047	0.6	22.6	2.5	3.1	0.07	98
109.	140325	839	13.96	23.441	0.9	70.516	1.0	19.1	1.4	3.2	0.11	111
110.	140326	2306	21.16	23.477	0.9	70.383	0.9	23.1	2	3.2	0.11	105
111.	140329	121	23.86	23.422	1.0	70.361	0.9	26.6	1.8	2.6	0.10	94
112.	140331	1047	6.31	23.468	0.9	70.372	1.4	26	2.4	2.5	0.05	136
113.	140401	833	11.12	23.481	0.8	70.289	0.7	17.7	2.5	2.4	0.04	105
114.	140401	1549	15.61	23.436	0.8	70.146	0.5	22.4	2.6	3.2	0.04	102
115.	140402	428	8.43	23.44	1.0	70.402	1.2	23.9	2.2	2.6	0.09	99
116.	140402	643	8.39	23.661	0.8	70.082	0.7	27	2.5	2.8	0.04	154
117.	140403	952	17.32	23.457	0.6	70.477	0.9	7.9	1.8	2.6	0.08	101
118.	140407	1857	48.64	23.057	0.9	69.667	1.0	16.1	1.0	2.6	0.06	129
119.	140409	1351	6.39	23.608	0.8	70.255	0.6	2.1	1.0	2.6	0.13	127
120.	140409	1715	40.24	23.312	1.3	70.106	0.8	27.4	1.8	3.0	0.15	76
121.	140410	543	21.6	23.386	1.1	70.348	0.9	30.1	1.5	3.0	0.07	99
122.	140410	950	34.86	23.448	1.0	70.361	0.9	18.1	2.4	3.2	0.11	99
123.	140410	1051	59.63	23.734	1.6	69.904	1.3	17.7	3.0	3.1	0.10	114
124.	140411	1313	47.81	23.327	1.2	70.356	0.9	31.3	1.3	3.2	0.05	127
125.	140411	1700	16.65	23.441	0.9	70.353	0.9	26.4	1.9	3.0	0.09	97
126.	140411	1809	11.45	23.453	0.8	70.264	0.7	18.4	2.5	2.6	0.05	100
127.	140412	1056	0.04	23.493	0.6	70.294	0.5	15	1.7	3.9	0.06	107
128.	140413	1156	37.4	23.449	1.0	70.299	1.2	21.3	3.4	2.8	0.10	105
129.	140414	112	22.06	23.479	0.9	70.204	1.1	15.5	2.8	2.4	0.08	114
130.	140414	347	4.23	23.342	1.1	70.374	0.9	20.5	1.5	3.5	0.08	135
131.	140415	3	16.67	23.514	0.8	70.116	0.6	2.0	1.0	3.8	0.16	101
132.	140417	112	3.58	23.417	1.6	70.418	1.4	26.3	2.7	2.3	0.17	110
133.	140419	315	40.07	23.474	1.0	70.438	1.1	21.1	1.7	2.5	0.10	91
134.	140419	614	17.15	23.731	0.9	70.381	0.8	34.2	1.7	2.7	0.04	156
135.	140419	2006	57.27	23.714	0.9	70.525	0.8	25.5	1.7	3.7	0.06	149
136.	140420	42	39.26	23.374	0.9	70.244	0.7	13.5	2.6	2.9	0.02	101
137.	140420	837	7.82	23.589	0.9	70.428	1.8	15.9	2.1	2.3	0.09	179
138.	140420	1644	7.18	23.37	1.1	70.238	0.9	33.1	1.9	3.7	0.10	104
139.	140426	19	52.01	23.427	0.8	70.179	0.6	21.6	2.7	3.0	0.04	95
140.	140427	253	47.21	23.543	0.7	70.315	0.6	8.3	1.8	2.8	0.06	116
141.	140428	19	23.23	23.372	1.1	70.392	1.0	26	1.6	3.6	0.09	129
142.	140428	59	29.34	23.531	0.9	70.525	0.9	21.6	1.2	3.0	0.06	106
143.	140428	1152	56.39	23.371	0.9	70.269	1.0	2.3	1.4	2.8	0.13	95
144.	140429	408	4.59	23.376	1.3	70.297	1.0	12	3.5	2.2	0.10	86
145.	140429	539	4.52	23.56	0.6	70.024	0.6	18.8	3.8	2.8	0.05	98
146.	140429	555	1.15	23.475	0.7	70.302	0.8	14.2	2.5	3.9	0.11	104
147.	140429	847	52.44	23.408	1.1	70.219	0.9	26	2.5	3.5	0.16	95
148.	140429	1522	47.01	23.38	0.9	70.258	0.7	14	2.1	3.5	0.13	95
149.	140501	127	32.03	23.437	1.0	70.359	1.7	20.2	3.1	2.4	0.02	139
150.	140501	840	41.5	23.553	0.6	70.126	0.5	17.2	4.4	2.7	0.06	108
151.	140501	1421	19.6	23.397	1.9	70.457	1.3	29	1.0	2.5	0.08	179
152.	140502	1421	51.72	23.563	0.7	70.092	0.6	10	2.5	2.8	0.07	127
153.	140502	1530	4.22	23.561	0.9	70.285	0.8	9.6	2.5	2.6	0.05	119
154.	140503	449	21.52	23.511	0.8	70.180	0.7	24.3	2.8	2.5	0.04	105

Table A1. *(Continued.)*

Sl. no.	Date (yymmdd)	Time (hhmm)	Time Sec	Latitude (°)	Error	Longitude (°)	Error	Depth (km)	Error	M_w	RMS	GAP
155.	140505	358	25.7	23.230	1.3	70.087	0.6	15.3	2.4	2.5	0.04	164
156.	140506	1046	20.07	23.550	0.8	70.071	0.7	28.5	3.2	2.5	0.03	121
157.	140506	1719	38.89	23.394	0.8	70.176	0.6	19.2	2.5	3.1	0.04	105
158.	140507	911	19.5	23.446	1.0	70.154	0.8	9.6	2.5	2.5	0.11	94
159.	140507	1057	50.63	23.581	1.1	70.482	1.1	15.6	1.3	3.1	0.04	122
160.	140507	1111	18.74	23.561	1.2	70.485	1.0	17	1.5	2.7	0.06	118
161.	140509	1035	48.3	23.490	0.7	70.437	1.0	15.5	1.4	3.2	0.08	97
162.	140509	1320	14.01	23.501	0.7	70.196	0.9	15.9	2.2	3.1	0.04	120
163.	140510	613	2.99	23.418	1.1	70.351	1.0	20.7	2.2	3.3	0.13	92
164.	140511	1026	0.15	23.424	0.8	70.461	0.9	21.1	1.3	3.2	0.05	121
165.	140512	1316	53.75	23.501	0.6	70.072	0.5	8.0	2.3	3.3	0.07	95
166.	140512	1423	53.75	23.585	0.7	70.090	0.5	18.7	3.7	2.9	0.05	111
167.	140512	1732	26.3	23.430	0.9	70.460	1.1	19.2	1.8	2.7	0.05	116
168.	140515	356	13.83	23.494	0.7	70.287	0.7	13.7	2.6	2.6	0.07	107
169.	140515	1146	47.28	23.471	0.9	70.390	1.0	17.9	2.0	2.7	0.07	102
170.	140518	1117	17.48	23.481	0.8	70.466	0.9	19.7	1.4	2.8	0.07	88
171.	140521	149	49.1	23.555	1.0	70.408	1.0	18.1	2	3.3	0.12	119
172.	140521	950	47.78	23.428	0.8	70.422	0.9	17.3	1.7	3.6	0.08	110
173.	140523	601	55.05	23.463	0.9	70.370	0.9	19.9	2.1	3.0	0.09	103
174.	140523	1121	28.1	23.476	0.8	70.119	0.7	32.4	2.8	2.8	0.07	96
175.	140525	408	53.26	23.416	1.1	70.293	1.0	31.3	2.0	3.4	0.09	96
176.	140525	745	4.12	23.447	0.8	70.268	0.7	10	1.7	2.6	0.10	99
177.	140526	756	29.2	23.399	1.0	70.425	1.0	27.7	1.3	2.8	0.08	127
178.	140527	552	33.79	23.618	1.7	70.553	1.2	32.4	2.1	2.7	0.07	126
179.	140527	1120	14.18	23.396	1.1	70.322	0.9	12.9	3.4	2.4	0.04	90
180.	140527	1341	47.68	23.295	1.1	70.145	0.7	25.2	2.2	3.2	0.05	145
181.	140527	2131	20.52	23.383	1.1	70.367	1.0	15.4	1.5	2.9	0.07	110
182.	140528	5	59.76	23.366	1.1	70.356	0.9	23.3	1.7	3.9	0.06	111
183.	140529	936	57.38	23.425	0.7	70.473	0.9	10.4	2.3	3.3	0.08	122
184.	140529	1619	59.71	23.456	0.9	70.318	0.8	21.8	2.1	3.5	0.04	102
185.	140530	1650	24.16	23.392	1.2	70.319	0.9	33	1.9	3.2	0.05	92
186.	140530	1806	50.73	23.351	1.0	70.393	0.9	10.0	1.4	3.0	0.04	141
187.	140603	1634	35.43	23.57	1.2	70.437	1.1	14.5	1.6	2.6	0.03	157
188.	140607	1046	50.14	23.431	1.1	70.187	0.8	31.9	2.3	3.3	0.09	94
189.	140608	645	30.58	23.38	1.2	70.349	1.0	30.1	1.5	3.0	0.06	102
190.	140608	1709	52.86	23.399	1.5	70.317	2.1	29.8	2.9	3.5	0.06	123
191.	140609	1641	50.52	23.483	0.7	70.201	0.6	20.2	2.5	2.6	0.04	102
192.	140610	22	52.49	23.52	0.9	70.469	0.9	19	1.4	3.1	0.09	96
193.	140610	523	34.65	23.47	0.7	70.144	0.5	18.8	2.9	2.8	0.04	97
194.	140611	403	31.53	23.454	0.8	70.534	1.0	15.1	1.1	3.6	0.09	95
195.	140611	537	24.61	23.305	1.5	70.331	0.9	12.4	1.7	2.6	0.06	113
196.	140612	312	15.74	23.337	1.1	70.32	0.9	9.6	1.5	3.8	0.07	87
197.	140612	1817	2.62	23.469	0.7	70.37	0.8	9.5	1.7	2.4	0.07	104
198.	140614	443	38.64	23.49	1.1	70.167	0.9	15.0	2.9	2.6	0.16	101
199.	140616	1823	13.53	23.348	1.0	70.306	0.8	24.1	1.5	2.8	0.05	87
200.	140617	631	26.24	23.749	1.0	70.622	1.1	16.3	2.7	2.6	0.06	156
201.	140618	443	13.08	23.709	0.9	70.407	0.8	27.2	1.7	2.6	0.05	152
202.	140618	1040	30.92	23.521	1.0	70.173	0.8	10.0	2.4	2.6	0.14	107
203.	140618	1255	50.11	23.45	0.7	70.094	0.5	15.3	1.9	3.3	0.06	97
204.	140619	829	15.87	23.489	0.8	70.425	0.8	17.7	1.5	3.0	0.09	101
205.	140619	1150	2.49	23.484	0.7	70.363	0.8	12.0	2.7	2.6	0.07	107
206.	140619	1434	2.4	23.48	0.9	70.385	0.8	26.4	1.6	2.8	0.07	106

Table A1. *(Continued.)*

Sl. no.	Date (yymmdd)	Time (hhmm)	Time Sec	Latitude (°)	Error	Longitude (°)	Error	Depth (km)	Error	M_w	RMS	GAP
207.	140619	1608	24.24	23.379	1.0	70.194	0.7	28.8	1.1	2.6	0.09	108
208.	140620	837	39.73	23.402	1.0	70.477	1.0	25.0	1.4	2.8	0.09	140
209.	140620	1044	23.09	23.379	0.9	70.218	0.6	13.0	2.9	2.8	0.03	104
210.	140622	234	1.96	23.364	1.2	70.315	0.8	13.8	2.3	3.1	0.07	84
211.	140622	933	20.15	23.631	1.1	70.43	0.8	23.1	1.7	2.7	0.08	134
212.	140622	1213	23.81	23.573	1.1	70.457	0.9	17.4	1.3	3.0	0.08	121
213.	140623	425	4.3	23.362	1.1	70.358	1.0	8.3	2	2.3	0.06	113
214.	140626	1505	55.31	23.401	0.8	70.402	0.8	11.5	2.3	2.7	0.08	118
215.	140628	636	44.86	23.393	2.1	70.305	1.3	33.0	2.9	3.5	0.01	113
216.	140628	2139	43.9	23.517	1.8	70.106	1.7	47.8	4.7	2.2	0.10	102
217.	140630	706	19.35	23.68	1.1	70.322	0.9	2.0	1.4	2.6	0.08	145
218.	140701	1137	47.48	23.39	1.1	70.466	1.3	24.8	1.9	2.73	0.03	146
219.	140703	756	34.93	23.367	1.0	70.362	0.9	9	1.7	2.94	0.08	114
220.	140704	1048	16.56	23.38	1.0	70.365	0.9	24.4	1.5	2.84	0.05	110
221.	140707	1132	4.48	23.336	1.2	70.37	1.0	20.2	1.6	2.32	0.06	135
222.	140707	2240	15.1	23.483	0.8	70.379	0.9	15.9	1.3	2.75	0.09	85
223.	140707	1927	17.09	23.488	0.8	70.466	0.9	19.40	1.4	2.62	0.08	106
224.	140712	215	49.15	23.428	1.0	70.413	1.0	23.3	1.7	2.99	0.09	108
225.	140712	1335	19.86	23.362	1.3	70.223	1.5	23.1	3.2	2.66	0.02	110
226.	140714	1724	41.55	23.35	1.1	70.406	0.9	24.8	1.4	2.82	0.05	150
227.	140716	304	27.48	23.396	1.2	70.345	1.0	31.5	1.6	3.46	0.07	95
228.	140716	1728	30.14	23.372	1.0	70.336	1.0	9.6	1.9	2.62	0.07	96
229.	140720	1616	19.81	23.643	1.0	70.391	0.9	27.9	1.7	2.97	0.10	137
230.	140722	45	36.38	23.463	1.0	70.417	1.0	24.4	1.7	3.05	0.09	92
231.	140722	838	28.55	23.371	0.9	70.153	0.6	21	2.5	3.01	0.05	115
232.	140723	351	37.27	23.48	0.9	70.493	1.1	15.8	1.4	2.66	0.06	108
233.	140724	236	14.47	23.368	0.9	70.065	0.6	22.4	2.9	3.06	0.06	118
234.	140728	1330	58.41	23.418	0.9	70.449	0.9	20.8	1.5	3.03	0.05	122
235.	140729	339	58.07	23.365	1.2	70.396	1.0	26.2	1.5	3.51	0.07	135
236.	140730	831	28	23.521	0.7	70.17	0.5	14.3	1.9	2.51	0.04	106
237.	140730	1049	59.57	23.38	1.1	70.343	1.0	25.3	1.9	2.91	0.05	98
238.	140802	6	8.89	23.357	1.1	70.375	0.9	21.9	1.5	3.07	0.05	127
239.	140802	249	49.83	23.358	1.2	70.39	1.2	32.6	1.7	2.95	0.03	136
240.	140803	1345	44.42	23.413	1.0	70.452	1.1	26.3	1.6	3.10	0.05	126
241.	140805	416	56.19	23.475	1.2	70.191	0.8	23.5	3.7	3.01	0.04	154
242.	140808	1551	18.82	23.514	0.8	70.097	0.6	15.8	2.1	2.69	0.03	117
243.	140809	436	49.69	23.47	0.9	70.151	0.6	24.4	3.3	3.18	0.02	127
244.	140812	1526	0.08	23.446	1.1	70.408	0.9	23.6	1.8	2.84	0.04	136
245.	140813	1009	27.15	23.419	1.1	70.371	0.9	20.2	2.2	3.02	0.04	146
246.	140813	1020	55.39	23.499	1.0	70.31	0.9	16.0	1.8	2.94	0.04	123
247.	140819	945	32.12	23.484	1.0	70.434	0.9	17.2	1.5	2.77	0.05	120
248.	140821	539	17.45	23.486	1.1	70.366	0.9	20.8	2.0	2.76	0.05	125
249.	140824	648	41.7	23.469	1.0	70.175	0.6	24.5	3.2	2.81	0.03	128
250.	140824	810	51.66	23.603	1.0	70.456	0.8	11.5	1.4	2.87	0.06	127
251.	140824	927	51.86	23.52	1.0	70.37	0.8	19.0	1.8	3.57	0.04	114
252.	140825	1215	44.53	23.505	1.1	70.302	0.8	19.5	2.8	2.88	0.05	121
253.	140825	1806	20.63	23.382	1.3	70.358	1.0	32.5	2.0	2.57	0.02	158
254.	140826	1600	52.28	23.554	0.9	70.305	0.7	12.2	3.3	3.00	0.03	118
255.	140827	255	44.32	23.679	1.1	70.421	0.9	28.7	1.3	3.89	0.04	144
256.	140827	926	56.19	23.374	1.3	70.191	0.7	28.8	1.5	3.12	0.04	150
257.	140827	1932	36.92	23.372	1.2	70.357	0.9	26.0	2.3	3.51	0.07	161
258.	140828	332	12.77	23.392	1.2	70.263	0.9	30.5	2.7	2.77	0.04	150

Table A1. *(Continued.)*

Sl. no.	Date (yymmdd)	Time (hhmm)	Time Sec	Latitude (°)	Error	Longitude (°)	Error	Depth (km)	Error	M_w	RMS	GAP
259.	140828	2249	50.25	23.473	1.1	70.398	0.9	22.3	1.7	2.55	0.04	142
260.	140829	853	2.75	23.807	1.9	69.942	2.0	8.3	3.3	2.60	0.02	166
261.	140831	45	24.16	23.353	1.1	70.236	0.6	9.9	2.1	3.13	0.03	158
262.	140901	2	25.59	23.410	1.2	70.371	0.9	25.3	2.1	2.7	0.04	149
263.	140903	354	7.59	23.111	0.9	69.745	2.3	18.0	3.0	2.4	0.04	152
264.	140904	14	12.65	23.472	1.1	70.401	0.9	23.9	1.7	2.6	0.05	127
265.	140904	817	32.23	23.460	1.3	70.458	1.1	29	0.8	2.7	0.05	127
266.	140905	1743	22.49	23.581	1.1	70.618	1.1	26	1.5	3.1	0.04	145
267.	140906	52	53.18	23.490	0.8	70.045	0.7	23.2	3.7	2.8	0.03	118
268.	140906	829	13.13	23.385	1.3	70.253	0.9	30.6	2.8	3.3	0.05	151
269.	140906	1032	46.69	23.500	0.9	70.581	1.0	11.0	1.7	2.8	0.09	135
270.	140907	1238	22.63	23.352	1.3	70.386	1.0	25.3	2.2	2.8	0.04	171
271.	140907	1735	47.02	23.355	1.3	70.168	0.7	27.2	2.0	3.0	0.05	153
272.	140907	2137	17.44	23.446	0.9	70.457	0.9	13.2	1.8	2.3	0.09	134
273.	140907	2331	36.55	23.442	1.1	70.302	0.8	26.0	2.3	2.3	0.05	138
274.	140913	1559	44.72	23.503	0.5	70.054	0.6	21.9	2.5	2.7	0.04	93
275.	140914	822	42.78	23.514	0.8	70.325	0.8	15.1	2.0	2.9	0.09	141
276.	140916	959	25.01	23.520	0.9	70.359	0.9	19.9	2.0	2.7	0.07	146
277.	140916	1057	7.92	23.416	0.7	70.143	0.6	17.3	2.2	2.9	0.05	121
278.	140920	1038	58.06	23.462	1.0	70.368	0.9	27.0	1.7	2.6	0.07	174
279.	140920	1836	37.8	23.398	0.9	70.244	0.8	34.0	1.4	3.7	0.06	160
280.	140921	1705	58.63	23.436	0.6	70.082	0.7	15.9	1.4	2.8	0.09	98
281.	140922	113	59.04	23.364	0.9	70.221	0.8	26.0	1.5	3.8	0.08	164
282.	140925	2125	12.46	23.390	0.8	70.178	0.7	25.6	1.6	2.4	0.07	139
283.	140926	2238	55.96	23.680	1.0	70.572	0.9	7.0	2.3	3.9	0.04	147
284.	140928	834	46.38	23.507	0.6	70.200	0.5	15.3	1.6	2.9	0.05	116
285.	140928	1813	22.9	23.476	0.5	70.077	0.5	13.8	2.2	2.9	0.04	93
286.	141001	1800	19.85	23.438	0.8	70.091	0.7	23.2	2.4	2.5	0.08	100
287.	141002	656	5.49	23.433	0.9	70.324	0.9	27.3	1.9	3.2	0.07	172
288.	141003	1613	9.99	23.102	0.8	69.715	1.1	26.4	1.2	3.7	0.08	142
289.	141004	943	6.42	23.488	0.9	70.29	0.8	15.3	1.6	3.2	0.11	143
290.	141004	1638	43.11	23.102	0.9	69.712	1.2	23.6	1.4	3.4	0.13	141
291.	141004	2044	20.06	23.504	1.0	70.329	0.9	20.1	2.3	2.4	0.06	146
292.	141005	851	29.08	23.51	0.9	70.438	0.8	16.6	1.2	3.2	0.05	176
293.	141008	453	41.29	23.519	1.1	70.462	1.0	21.0	1.3	3.2	0.07	178
294.	141009	432	31.36	23.444	1.0	70.346	1.0	29.1	1.5	3.1	0.06	174
295.	141010	915	11.2	23.612	0.8	69.99	1.0	28	2.2	2.8	0.10	101
296.	141011	1753	4.21	23.594	1.0	70.411	1.0	15.1	1.6	2.7	0.08	126
297.	141012	102	49.57	23.524	0.7	70.157	0.6	24.5	2.5	2.9	0.04	106
298.	141013	230	32.16	23.511	0.6	70.159	0.5	14.0	2.6	2.8	0.04	107
299.	141014	1334	21.3	23.405	1.1	70.213	0.9	36.0	2.0	3.3	0.08	148
300.	141018	1914	10.15	23.565	0.8	70.058	0.9	21.3	4.0	3.7	0.15	103
301.	141018	2224	5.21	23.482	0.6	70.12	0.6	31.7	1.9	3.7	0.04	102
302.	141024	306	1.8	23.476	0.5	70.077	0.6	21.0	2.4	2.8	0.04	93
303.	141024	1511	0.73	23.355	1.1	70.192	0.9	30.4	1.6	2.6	0.06	156
304.	141025	1614	14.59	23.457	0.9	70.227	0.8	35.1	2.0	3.0	0.07	137
305.	141025	1916	33.14	23.649	0.8	70.286	0.6	9.40	1.6	3.0	0.06	137
306.	141028	1913	49.72	23.523	1.2	70.401	1.0	22.2	1.8	3.9	0.08	155
307.	141030	904	50.79	23.579	0.5	70.057	0.6	24.5	2.4	3.8	0.05	106
308.	141104	839	46.62	23.411	1.0	70.3	1.0	18.0	2.5	2.6	0.03	173
309.	141105	34	20.05	23.657	1.0	70.388	0.8	24.8	2.0	3.0	0.04	140
310.	141113	2119	47.8	23.379	1.0	70.249	0.9	19.9	2.3	2.8	0.07	169

Table A1. *(Continued.)*

Sl. no.	Date (yymmdd)	Time (hhmm)	Time Sec	Latitude (°)	Error	Longitude (°)	Error	Depth (km)	Error	M_w	RMS	GAP
311.	141115	514	12.97	23.439	1.0	70.247	0.8	31.3	1.9	2.7	0.05	148
312.	141115	854	30.5	23.429	1.3	70.361	1.3	28.9	1.0	2.7	0.05	180
313.	141115	1041	30.5	23.521	1.1	70.453	0.9	22.6	1.2	3.3	0.04	176
314.	141122	611	57.65	23.484	0.8	70.154	0.8	31.2	2.4	3.0	0.05	111
315.	141123	1127	39.75	23.503	0.6	70.114	0.6	14.1	2.9	2.9	0.03	99
316.	141123	1300	23.82	23.583	1.0	70.382	0.8	25.9	1.8	3.3	0.07	124
317.	141128	419	10.83	23.463	1.3	70.363	1.0	28.8	1.0	2.7	0.05	173
318.	141128	1229	42.47	23.532	0.6	70.191	0.6	21.6	2.5	2.9	0.04	110
319.	141129	1733	3.29	23.541	1.0	70.128	0.9	14.5	3.5	2.8	0.02	133
320.	141129	2332	20.36	23.532	1.2	70.444	1.0	20.7	1.4	2.9	0.03	164
321.	141202	343	39.29	23.513	0.8	70.204	0.7	22.3	2.8	2.8	0.05	116
322.	141204	618	18.91	23.37	0.8	70.154	0.7	21.9	1.7	3.1	0.04	134
323.	141204	1320	4.17	23.541	1.1	70.461	0.9	19.5	1.2	2.6	0.05	165
324.	141206	840	31.08	23.799	0.9	69.925	0.8	7.1	1.7	2.7	0.09	151
325.	141208	1551	43.1	23.514	1.1	70.405	0.9	16	1.1	2.9	0.04	162
326.	141210	1434	54.39	23.523	0.7	70.15	0.6	27.8	2.4	2.5	0.03	105
327.	141213	521	5.75	23.622	0.8	70.059	0.9	27.6	1.9	2.8	0.08	115
328.	141215	1704	4.69	23.45	1.1	70.347	0.9	26.4	1.9	2.9	0.07	173
329.	141219	825	28.45	23.515	0.8	70.272	0.7	19.6	2.4	2.9	0.05	129
330.	141221	1005	24.62	23.38	1.2	70.251	0.8	22.6	2.2	3.1	0.05	169
331.	141222	2029	6.52	23.488	0.8	70.131	0.7	27.6	1.7	2.6	0.07	105
332.	141224	423	17.71	23.566	0.7	70.071	0.8	23.2	3.4	2.9	0.09	105
333.	141225	123	0.39	23.458	0.9	70.105	0.8	29.0	1.9	3.3	0.09	102
334.	141226	1417	28.51	23.511	1.0	70.333	0.9	17.3	2.5	3.1	0.07	144
335.	141228	323	18.69	23.585	1.3	70.513	0.9	11.6	1.2	2.8	0.04	151
336.	141229	616	53.27	23.541	1.0	70.271	0.9	16.1	1.9	3.1	0.09	120
337.	150103	157	24.26	23.566	0.5	70.056	0.6	14.9	2.9	2.8	0.05	103
338.	150105	1721	19.52	23.393	1.1	70.256	0.8	16.7	2.5	3.6	0.05	166
339.	150107	1022	29.8	23.657	0.8	70.537	0.7	5.3	2.5	3.1	0.06	138
340.	150108	130	56.09	23.521	0.6	70.123	0.6	15.4	2.5	3.5	0.04	103

Table A2. *Hypocentral parameters of aftershock events which have used for estimation of source parameters.*

Sl. no.	Date (yymmdd)	Time (hh:mm)	Latitude (°)	Longitude (°)	Depth (km)	Magnitude (M_w)
1.	140501	01:27	23.44	70.36	20.2	2.4
2.	140501	08:40	23.55	70.13	17.2	2.7
3.	140501	14:21	23.40	70.46	29.0	2.5
4.	140502	14:21	23.56	70.09	10.0	2.8
5.	140502	15:30	23.56	70.28	09.6	2.6
6.	140503	04:49	23.51	70.18	24.3	2.5
7.	140503	09:36	23.39	70.20	01.2	2.7
8.	140503	16:12	23.36	70.40	23.4	2.4
9.	140505	03:58	23.23	70.09	15.3	2.5
10.	140506	10:46	23.55	70.07	28.5	2.5
11.	140506	17:19	23.39	70.18	19.2	3.1
12.	140507	09:11	23.45	70.15	09.6	2.5
13.	140507	10:57	23.58	70.48	15.6	3.1
14.	140507	11:11	23.56	70.49	17.0	2.7
15.	140509	02:02	23.92	70.35	25.3	3.1
16.	140509	10:35	23.49	70.44	15.5	3.2

Table A2. *(Continued.)*

Sl. no.	Date (yymmdd)	Time (hh:mm)	Latitude (°)	Longitude (°)	Depth (km)	Magnitude (M_w)
17.	140509	13:20	23.50	70.20	15.9	3.1
18.	140510	06:13	23.42	70.35	20.7	3.3
19.	140511	10:26	23.42	70.46	21.1	3.2
20.	140512	13:16	23.50	70.07	08.0	3.3
21.	140512	14:23	23.58	70.09	18.7	2.9
22.	140512	17:32	23.43	70.46	19.2	2.7
23.	140515	03:56	23.49	70.29	13.7	2.6
24.	140515	11:46	23.47	70.39	17.9	2.7
25.	140518	11:17	23.48	70.47	19.7	2.8
26.	140521	01:49	23.55	70.41	18.1	3.3
27.	140521	09:50	23.43	70.42	17.3	3.6
28.	140523	06:01	23.46	70.37	19.9	3.0
29.	140523	11:21	23.48	70.12	32.4	2.8
30.	140525	04:08	23.42	70.29	31.3	3.4
31.	140525	07:45	23.45	70.27	10.0	2.6
32.	140526	07:56	23.40	70.42	27.7	2.8
33.	140527	05:52	23.62	70.55	32.4	2.7
34.	140527	11:20	23.40	70.32	12.9	2.4
35.	140527	11:23	23.72	70.80	21.9	3.5
36.	140527	13:41	23.30	70.14	25.2	3.2
37.	140527	21:31	23.38	70.37	15.4	2.9
38.	140528	05:00	23.37	70.36	23.3	3.9
39.	140529	09:36	23.42	70.47	10.4	3.3
40.	140529	16:19	23.46	70.32	21.8	3.5
41.	140530	16:50	23.39	70.32	33.0	3.2
42.	140530	18:06	23.35	70.39	10.0	3.0
43.	140531	08:40	23.91	70.06	02.4	2.6
44.	140531	15:38	23.90	70.11	25.0	3.2
45.	140606	16:14	23.43	70.58	31.6	2.2
46.	140607	10:46	23.43	70.19	31.9	3.3
47.	140608	06:45	23.38	70.35	30.1	3.0
48.	140608	17:09	23.40	70.32	29.8	3.5
49.	140609	16:41	23.48	70.20	20.2	2.6
50.	140610	00:22	23.52	70.47	19.0	3.1
51.	140610	05:23	23.47	70.14	18.8	2.8
52.	140611	04:03	23.45	70.53	15.1	3.6
53.	140611	05:37	23.31	70.33	12.4	2.6
54.	140612	03:12	23.34	70.32	09.6	3.8
55.	140612	18:17	23.47	70.37	09.5	2.4
56.	140614	04:43	23.49	70.17	15.0	2.6
57.	140614	17:10	23.27	70.41	23.2	3.0
58.	140615	18:17	23.15	70.33	30.0	2.7
59.	140616	18:23	23.35	70.31	24.1	2.8
60.	140617	06:31	23.75	70.62	16.3	2.6
61.	140618	04:43	23.71	70.41	27.2	2.6
62.	140618	10:40	23.52	70.17	10.0	2.6
63.	140618	12:55	23.45	70.09	15.3	3.3
64.	140619	08:29	23.49	70.42	17.7	3.0
65.	140619	11:50	23.48	70.36	12.0	2.6
66.	140619	14:34	23.48	70.38	26.4	2.8
67.	140619	16:08	23.38	70.19	28.8	2.6
68.	140620	08:37	23.40	70.48	25.0	2.8
69.	140620	10:44	23.38	70.22	13.0	2.8

Table A2. *(Continued.)*

Sl. no.	Date (yymmdd)	Time (hh:mm)	Latitude (°)	Longitude (°)	Depth (km)	Magnitude (M_w)
70.	140620	12:35	23.56	69.68	32.5	2.4
71.	140622	02:34	23.36	70.31	13.8	3.1
72.	140622	09:33	23.63	70.43	23.1	2.7
73.	140622	12:13	23.57	70.46	17.4	3.0
74.	140623	04:25	23.36	70.36	08.3	2.3
75.	140626	15:05	23.40	70.40	11.5	2.7
76.	140628	06:36	23.39	70.31	33.0	3.5
77.	140629	21:39	23.87	70.56	36.9	2.3
78.	140630	07:06	23.64	70.28	28.8	2.6

Table A3. *Source parameters of 78 aftershock events which have occurred during May–June 2014.*

Sl. no.	Corner frequency (f_c)	Standard deviation (σ_{f_c})	Seismic moment (M_0)	Standard deviation ($\sigma_{\log(M_0)}$)	Error factor (E_{mo})	Source radius (r)	Standard deviation (σ_r)	Stress drop (Std)	Standard deviation (σ_{Std})
1.	8.7	0.2	6.1E+12	0.27	1.32	148.8	2.8	0.08	0.04
2.	8.1	0.7	3.2E+13	0.69	1.99	160.9	14.2	0.27	0.31
3.	8.6	0.4	9.6E+12	0.44	1.55	151.7	7.1	0.11	0.09
4.	7.8	1.1	5.9E+13	0.93	2.53	168.6	25.6	0.36	0.42
5.	7.9	0.4	2.5E+13	0.43	1.54	163.7	8.5	0.23	0.24
6.	8.5	0.8	1.1E+13	0.46	1.59	152.5	12.6	0.12	0.11
7.	7.9	0.9	3.5E+13	0.64	1.89	166.6	19.4	0.24	0.32
8.	8.5	0.5	6.5E+12	0.28	1.33	152.5	8.5	0.08	0.05
9.	8.5	0.4	9.3E+12	0.42	1.52	153.4	6.8	0.10	0.09
10.	8.5	0.8	1.2E+13	0.62	1.86	152.7	14.9	0.12	0.12
11.	7.3	1.4	3.1E+14	1.15	3.15	182.9	37.6	1.18	1.61
12.	8.4	0.5	1.2E+13	0.52	1.67	154.4	8.4	0.12	0.13
13.	7.1	0.7	7.5E+13	0.47	1.60	183.2	17.9	0.46	0.34
14.	8.0	0.6	1.9E+13	0.47	1.60	162.2	11.6	0.18	0.12
15.	7.2	1.5	2.1E+14	0.97	2.63	186.8	38.7	0.85	0.89
16.	7.0	0.9	6.9E+13	0.41	1.50	197.7	30.3	0.83	0.73
17.	7.3	1.5	1.3E+14	0.95	2.59	183.1	33.9	0.69	0.74
18.	6.9	1.9	9.5E+14	1.50	4.47	200.1	55.2	2.70	3.23
19.	7.1	1.0	1.3E+14	0.60	1.83	185.9	24.3	0.76	0.72
20.	6.9	1.0	2.4E+14	0.66	1.94	192.4	29.5	1.07	0.92
21.	7.7	1.0	1.3E+14	1.01	2.75	170.3	23.3	0.78	1.11
22.	7.9	0.2	1.8E+13	0.30	1.35	163.7	3.5	0.18	0.14
23.	8.2	0.6	2.7E+13	0.65	1.91	159.4	12.2	0.23	0.31
24.	8.1	0.3	1.6E+13	0.40	1.49	161.0	5.9	0.16	0.13
25.	8.1	0.9	3.4E+13	0.62	1.86	161.9	16.3	0.30	0.25
26.	7.0	0.6	2.4E+14	0.65	1.91	185.2	15.2	1.37	1.48
27.	6.6	0.5	3.0E+14	0.27	1.32	197.2	14.5	1.68	0.86
28.	7.5	0.7	7.5E+13	0.50	1.65	173.8	18.1	0.49	0.46
29.	8.2	0.5	2.3E+13	0.37	1.44	157.9	10.1	0.23	0.18
30.	6.7	0.7	2.5E+14	0.52	1.69	193.8	19.0	1.26	1.14
31.	8.3	0.7	2.4E+13	0.76	2.15	157.3	13.4	0.22	0.24
32.	8.0	0.4	2.7E+13	0.40	1.49	162.9	9.1	0.24	0.24
33.	8.2	0.3	1.7E+13	0.44	1.56	158.3	6.4	0.18	0.12
34.	8.3	0.3	8.6E+12	0.49	1.63	156.1	4.9	0.09	0.09
35.	6.4	0.7	2.9E+14	0.49	1.64	204.4	21.9	1.42	1.05
36.	7.4	0.8	1.7E+14	0.70	2.02	177.2	20.2	1.00	1.15

Table A3. *(Continued.)*

Sl. no.	Corner frequency (f_c)	Standard deviation (σ_{f_c})	Seismic moment (M_0)	Standard deviation ($\sigma_{\log(M_0)}$)	Error factor (E_{mo})	Source radius (r)	Standard deviation (σ_r)	Stress drop (Std)	Standard deviation (σ_{Std})
37.	7.8	0.1	2.9E+13	0.23	0.23	166.9	3.0	0.27	0.13
38.	5.3	1.8	3.2E+15	1.22	1.26	262.6	63.3	5.73	4.46
39.	6.6	0.5	1.5E+14	0.47	1.59	198.1	14.0	0.84	0.59
40.	6.3	0.1	2.2E+14	0.28	1.33	205.2	4.7	1.11	0.63
41.	7.1	0.7	1.6E+14	0.69	1.99	183.1	18.1	0.90	0.92
42.	7.2	0.7	8.1E+13	0.62	1.85	182.6	19.5	0.50	0.54
43.	7.9	1.7	4.3E+13	1.32	3.76	166.8	35.9	0.27	0.35
44.	7.4	0.8	1.2E+14	0.54	1.72	177.4	19.5	0.76	0.62
45.	8.9	0.3	2.7E+12	0.34	1.40	146.0	4.5	0.04	0.02
46.	6.8	1.5	4.1E+14	1.01	2.76	197.0	42.8	1.31	1.49
47.	7.5	0.7	9.1E+13	0.53	1.69	173.8	17.2	0.58	0.62
48.	6.5	0.7	2.9E+14	0.38	1.46	201.5	20.2	1.31	1.00
49.	8.2	0.4	1.4E+13	0.33	1.40	158.9	7.5	0.14	0.08
50.	7.3	0.9	6.8E+13	0.43	1.54	179.8	22.1	0.43	0.30
51.	7.9	0.8	4.6E+13	0.64	1.90	166.0	18.0	0.34	0.35
52.	6.0	1.0	4.7E+14	0.39	1.48	219.5	33.7	1.63	1.09
53.	8.1	0.6	1.8E+13	0.50	1.64	160.8	11.0	0.17	0.14
54.	5.6	1.0	9.5E+14	0.58	1.78	238.4	46.4	2.27	1.63
55.	8.5	0.2	4.9E+12	0.22	1.25	152.1	3.5	0.06	0.03
56.	8.2	0.7	2.0E+13	0.57	1.78	159.5	13.0	0.18	0.19
57.	7.7	0.3	4.9E+13	0.38	1.46	169.2	5.8	0.42	0.33
58.	8.0	0.4	2.3E+13	0.39	1.48	162.0	7.0	0.22	0.21
59.	7.8	0.8	6.3E+13	0.76	2.13	168.4	20.1	0.38	0.56
60.	8.3	0.6	1.2E+13	0.45	1.58	156.0	10.2	0.13	0.09
61.	8.4	0.7	1.4E+13	0.47	1.61	155.5	11.7	0.15	0.13
62.	8.2	0.2	1.1E+13	0.19	1.21	158.3	4.8	0.11	0.04
63.	7.0	0.5	1.5E+14	0.48	1.61	186.1	13.5	0.93	0.69
64.	7.5	0.3	5.5E+13	0.38	1.46	173.1	6.8	0.44	0.31
65.	8.2	0.3	1.1E+13	0.33	1.39	157.3	4.7	0.12	0.08
66.	7.9	0.4	2.8E+13	0.50	1.65	164.0	8.9	0.25	0.23
67.	8.1	0.2	1.3E+13	0.31	1.36	160.1	4.8	0.14	0.09
68.	7.9	0.4	2.6E+13	0.34	1.40	165.2	7.5	0.24	0.16
69.	7.6	1.0	4.3E+13	0.58	1.78	172.1	23.3	0.29	0.29
70.	8.9	1.2	1.1E+13	0.76	2.15	146.3	18.7	0.12	0.16
71.	7.0	0.7	8.0E+13	0.42	1.52	185.5	17.7	0.47	0.48
72.	7.9	0.5	2.2E+13	0.35	1.42	163.5	9.7	0.20	0.17
73.	7.2	0.8	8.8E+13	0.60	1.82	181.3	20.7	0.50	0.50
74.	8.4	0.4	5.5E+12	0.37	1.45	154.4	7.8	0.06	0.06
75.	7.9	0.4	1.9E+13	0.28	1.32	165.2	7.2	0.18	0.12
76.	6.2	0.3	3.0E+14	0.58	1.78	207.8	9.9	1.36	1.32
77.	8.8	0.1	3.0E+12	0.05	1.05	147.3	2.1	0.04	0.01
78.	8.4	0.2	8.8E+12	0.18	1.20	154.3	3.7	0.10	0.04

References

Aki K 1962 Revision of some results obtained in the study of the source function of Rayleigh waves*; J. Geophys. Res.* **67** 3645–3647.

Antolik M and Dreger D S 2003 Rupture process of the 26 January 2001 M_w 7.6 Bhuj, India, earthquake from teleseismic broadband data; *Bull. Seismol. Soc. Am.* **93** 1235–1248.

Archuleta R J, Cranswick E, Muellar C and Spudich P 1982 Source parameters of the 1980 Mammoth Lakes, California, earthquake sequence; *J. Geophys. Res.* **87** 4595–4607.

Baumbach M, Grosser H, Schmidt H G, Paulat A, Rietbrock A, Rao C V R K, Soloman Raju P, Sarkar D and Mohan 1994 Study of the foreshocks and aftershocks of the intraplate Latur earthquake of September 30, 1993, India; *Geol. Soc. India Memoir* **35** 33–63.

Biswas S K 1987 Regional tectonic framework, structure, and evolution of the marginal western basins of India; *Tectonophys.* **135** 307–327.

Biswas S K 2005 A review of structure and tectonics of Kutch Basin, Western India, with special reference to earthquakes; *Curr. Sci.* **88(10)** 15.

Biswas S K and Khattri K N 2003 Structure and tectonics of Kutch Basin, western India, with special reference to earthquake; *J. Geol. Soc. India* **61** 626–629.

Boatwright J 1980 A spectral theory for circular seismic sources; simple estimates of source dimension, dynamic stress drop, and radiated seismic energy; *Bull. Seismol. Soc. Am.* **70** 1–27.

Bodin P, Malagnini L and Akinci A 2004 Ground-motion scaling in the Kachchh basin, India, deduced from aftershocks of the 2001 M_w 7.6 Bhuj earthquake; *Bull. Seismol. Soc. Am.* **94** 1658–1669.

Bott M H P and Dean D S 1973 Stress diffusion from plate boundaries; *Nature* **243** 339–341.

Brune J N 1970 Tectonic stress and spectra of seismic shear waves from earthquakes; *J. Geophys. Res.* **75** 4997–5009.

Fletcher J, Boatwright J, Haar L, Hanks T and McGarr A 1984 Source parameters for aftershocks of the Oroville, California, earthquake; *Bull. Seismol. Soc. Am.* **74** 1101–1123.

Fletcher J B 1995 Source parameters and crustal Q for four earthquakes in South Carolina; *Seismol. Res. Lett.* **66** 44–58.

Gupta H K, Rao N P, Rastogi B K and Sarkar D 2001 Bhuj earthquake of 26 January 2001; *J. Geol. Soc. India* **57** 275–278.

Johnston A C 1994 Seismotectonic interpretations and conclusions from the stable continental regions; In: *The Earthquakes of Stable Continental Regions: Assessment of Large Earthquakes Potential*, Electrical Power and Research Institute, Palo Alto, Report TR 10261 (Chapter 3).

Jordan T H and Sverdrup K A 1981 Teleseismic location techniques and their application to earthquake clusters in the South-Central Pacific; *Bull. Seismol. Soc. Am.* **71** 1105–1130.

Kanamori H and Allen C R 1986 Earthquake repeat time and average stress drop; *Am. Geophys. Monogr.* **37** 227–235.

Keilis-Borok V I 1959 An estimation of the displacement in an earthquake source and of source dimensions; *Ann. Geofis.* **12** 205–214.

Kumar M, Yallanki V S, Biswas K and Mandal P 2015 Evidence for non-self-similarity in the M_w 7.7 2001 Bhuj earthquake sequence; *Nat. Hazards* **75(2)** 1577–1598.

Kumar S, Kumar D and Rastogi B K 2014 Source parameters and scaling relations for small earthquakes in the Kachchh region of Gujarat, India; *Nat. Hazards* **73** 1269–1289.

Mandal P 2007 Sediment thickness and Q_s *vs.* Q_p relations in the Kachchh rift basin, Gujarat, India, using Sp converted phases; *Pure Appl. Geophys.* **164** 135–160.

Mandal P, Satyamurty C and Raju I P 2009 Iterative deconvolution of the local waveforms: characterization of the seismic sources in Kachchh, India; *Tectonophys.* **478(3)** 143–157.

Mandal P and Johnston A 2006 Estimation of source parameters for the aftershocks of the 2001 M_w 7.7 Bhuj earthquake, India; *Pure Appl. Geophys.* **163** 1537–1560.

Mandal P and Dutta U 2011 Estimation of earthquake source parameters and site response; *Bull. Seismol. Soc. Am.* **101(4)** 1719–1731.

Mandal P, Kumar M and Biswas K 2016 Evidence for a fluid flow triggered spatio-temporal migration of seismicity in the 2001 M_w 7.7 Bhuj earthquake region, Gujarat, India, during 2001–2013; *J. Earth Syst. Sci.* **125(6)** 1285–1298.

Mandal P and Pandey O P 2010 Relocation of aftershocks of the 2001 Bhuj earthquake: A new insight into seismotectonics of the Kachchh seismic zone, Gujarat, India; *J. Geodyn.* **49** 254–260.

Mandal P and Rastogi B K 2005 Self-organized fractal seismicity and b value of aftershocks of the 2001 Bhuj earthquake in Kutch (India); *Pure Appl. Geophys.* **162(1)** 53–72.

Mandal P, Rastogi B K and Sarma C S P 1998 Source parameters of Koyna Earthquakes, India; *Bull. Seismol. Soc. Am.* **88(3)** 833–842.

Mandal P, Srivastava J, Joshi S, Kumar S, Bhunia R and Rastogi B K 2004a Low coda-Q_c in the epicentral region of the 2001 Bhuj Earthquake of M_w 7.7; *Pure Appl. Geophys.* **161** 1635–1654.

Mandal P, Rastogi B K, Satyanarayana H V S, Kousalya M, Vijayraghavan R, Satyamurthy C, Raju I P, Sarma A N S and Kumar N 2004b Characterization of the causative fault system for the 2001 Bhuj earthquake of M_w 7.7; *Tectonophys.* **378** 105–121.

Mayeda K and Walter W R 1996 Moment, energy, stress drop, and source spectra of western United States earthquakes from regional coda envelopes; *J. Geophys. Res.* **101(B510)** 11,195–11,208.

Mishra P K 2004 The Kutch Earthquake 2001, New Delhi, India; *National Institute of Disaster Management, Ministry of Home Affairs, Government of India.* **Chapter 3**, 56p.

Nagamani D and Mandal P 2017 Estimation of earthquake source parameters in the Kachchh seismic zone, Gujarat, India, using three component S-wave spectra; *J. Earth Syst. Sci.* **126(5)** 74.

Press W H, Teukolsky S A, Vetterling W T and Flannery B P 1992 *Numerical recipes in FORTRAN and C*; Academic Press, New York, 382p.

Rapolu N and Mandal P 2014 Source parameters of the 2001 M_w 7.7 Bhuj earthquake, Gujarat, India, aftershock sequence; *J. Geol. Soc. India* **83(5)** 517–531.

Rastogi B K 2001 Ground deformation study of M_w 7.7 Bhuj earthquake of 2001; *Episodes* **24(3)** 160–165.

Rastogi B K, Kumar S, Aggrawal S K, Mohan K, Rao P, Rao N and Ch Kothyari G 2013a The October 20, 2011 M_w 5.1 Talala earthquake in the stable continental region of India; *Nat. Hazards* **65(2)** 1197–1216.

Rastogi B K, Aggrawal S K, Rao N and Choudhury P 2013b Triggered/migrated seismicity due to the 2001 M_w 7. 7 Bhuj earthquake, western India; *Nat. Hazards* **65(2)** 1085–1107.

Rastogi B K, Mandal P and Biswas S K 2014 *Intraplate earthquakes, Pradeep Talwani, Cambridge*; Cambridge University Press, **Chapter 6**, pp. 126–161.

Saha A, Lijesh S and Mandal P 2012 Simultaneous estimation of earthquake source parameters and crustal Q value from broadband data of selected aftershocks of the 2001 M_w 7.7 Bhuj earthquake; *J. Earth Syst. Sci.* **121** 1421–1440.

Seismic Analysis Code (SAC) 2000 (http://www.iris.edu/manuals/sac/SAC_Home_Main.html), 280p.

Sairam B, Singh A P and Kumar M R 2018 Comparison of earthquake source characteristics in the Kachchh Rift Basin and Saurashtra horst, Deccan Volcanic Province, western India. *J. Earth Syst. Sci.* **127** 55.

Savage J C 1971 A theory of creep waves propagating along a transform fault; *J. Geophys. Res.* **76(8)** 1954–1966.

Scholz C H 1977 A physical interpretation of the Haicheng earthquake prediction; *Nature* **267** 121–124.

Scholz C H, Aviles C and Wesnousky S 1986 Scaling differences between large intraplate and interpolate earthquakes; *Bull. Seismol. Soc. Am.* **76** 65–70.

Singh S K, Dattatrayam R S, Shapiro N M, Mandal P, Pacheco J F and Midha R K 1999 Crustal and Upper Mantle structure of Peninsular India and Source Parameters of the May 21, 1997, Jabalpur Earthquake ($M_w = 5.8$): Results from a New Regional Broad-band Network; *Bull. Seismol. Soc. Am.* **89** 1632–1641.

Singh S K, Pacheco J F, Bansal B K, Perez-campos X, Dattatrayam R S and Suresh G 2004 A source study of the Bhuj, India Earthquake of 26 January 2001 ($M_w = 7.6$); *Bull. Seismol. Soc. Am.* **94** 1195–1206.

Toro G R and Silva W J 2001 Scenario earthquakes for Saint Louis, MO and Memphis, TN and seismic hazard maps for the Central United States region including the effect of site conditions; In: *US Geological Survey Final Technical Report* 1434-HQ-97-GR-02981, 248p.

Trivedi P C and Parvez I A 2015 Characterization of source parameters and some empirical relations between them for Kachchh Region, Gujarat, India: Implication of January 26, 2001 Bhuj Earthquake and its aftershock sequence; *Int. J. Geosci.* **6** 1127–1139.

Corresponding editor: M Radhakrishna